

Journal of MARINE RESEARCH

Volume 59, Number 4

On the summer mesoscale variability of the Black Sea

by Şükürü T. Beşiktepe¹, Carlos J. Lozano² and Allan R. Robinson²

ABSTRACT

The evolution of the Black Sea temperature, salinity and circulation, from large scale to mesoscale, is studied using a data-driven primitive equation simulation. The data are drawn from (i) a basin-wide hydrographic survey, CoMSBlack'92, obtained in the Summer of 1992; (ii) wind stress derived from wind analyses of the Sevastopol MSIA/URHI Office; (iii) climatological heat fluxes; and (iv) climatological river outflows. The primitive equation model is from the Harvard Ocean Prediction System. The simulation is used to examine the evolution of the circulation at mesoscale resolution, its dominant variabilities and dependencies in the summer period. The large-scale upper layer circulation over the deep portion of the basin is generally cyclonic with a system of anticyclonic eddies evolving in its periphery. The edge of the cyclonic circulation is dominated by an inertial jet: the Rim Current. As the Rim Current transverses the edge of the deep basin, the meandering and secondary circulation associated to the jet varies according to internal dynamics and interactions with the bottom topography and shelf water circulation. The relatively broad northwestern shelf is found to be mostly wind driven with a buoyancy-driven coastal current and interacting with the quasi-stationary Crimea and Kaliakra anticyclones. The seasonal thermocline is strengthened during this period and a zonal large-scale temperature gradient with warmer/colder sea-surface temperatures in the east/west is driven by the observed weak/strong winds. Some of the major circulation elements are partially verified using qualitative comparisons with the Summer of 1992 data and historical data; both *in situ*, and infrared and color remotely sensed data. The Rim Current meander shape and propagation parameters, eddy size and distribution, and the generation of rapid surface bound jets are found to be in good agreement with observations. The simulation shows two previously unobserved events: an anticyclonic eddy is shed near Sinop; and the anticyclones moving north along the Caucasian coast are formed and shed from the Batumi eddy. Imprints of these events are found in the historical record.

1. Institute of Marine Sciences, Middle East Technical University, P.O. Box 28 Erdemli, İçel 33731, Turkey.
email: sukru@ims.metu.edu.tr

2. Harvard University, Division of Engineering and Applied Sciences, Cambridge, Massachusetts, 02138, U.S.A.

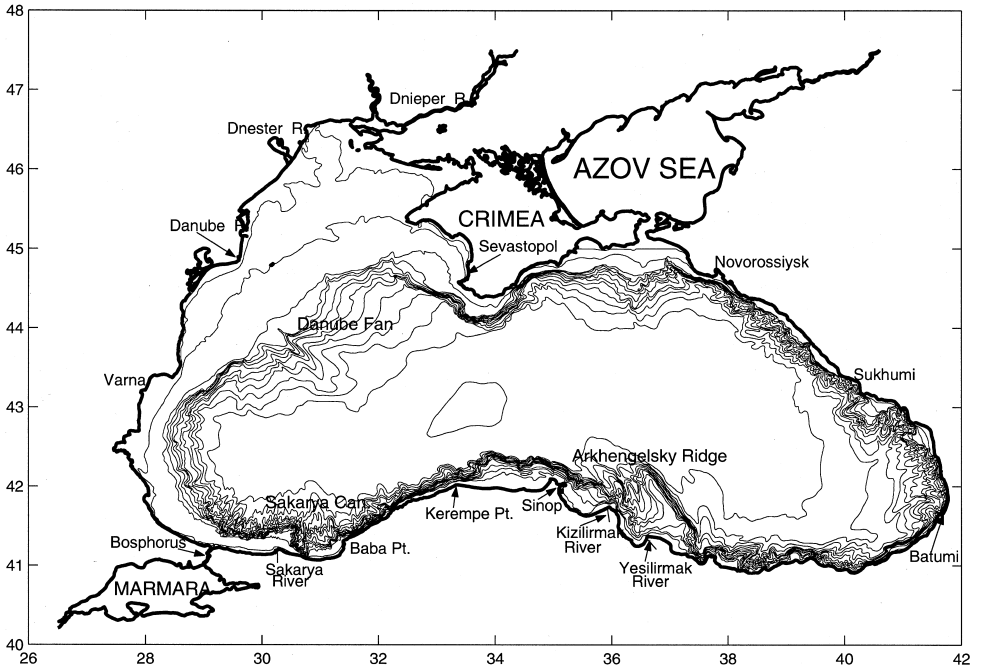


Figure 1. Black Sea topography (after IOC). Contour intervals in meters 10, 20, 50, 100 (dark) and [200:200:2200] (light). Geographical locations, topographic features and rivers mentioned in the text are also shown.

1. Introduction

In recent years, substantive observational and modeling efforts have increased our knowledge of the physical oceanography in the Black Sea. For an overview see for instance: Ünlüata *et al.* (1993); summaries and initial studies based upon basin-wide hydrographic surveys conducted in the summers of 1991 (HydroBlack91), 1992 (CoMS-Black92), and 1993 (CoMS-Black93); remotely sensed and *in situ* historical data (Oğuz *et al.*, 1992; 1993; 1994; Oğuz and Beşiktepe, 1999). These studies provide an initial coherent description of the basin and sub-basin circulation and its variability. The overall state of knowledge on the Black Sea physical oceanography can be found in the monographs and review papers (Filippov, 1966; Blatov *et al.*, 1984; Stanev, 1990; Özsoy and Ünlüata, 1998) and references therein.

The large-scale circulation of the Black Sea includes a deep basin circulation and the circulation on the shelves. The deep basin circulation includes cyclonic eddies embedded in a large cyclonic central circulation. In the periphery of the central circulation a complex of anticyclonic eddies are linked, most of the time, by a meandering and highly variable current moving counter-clockwise around the basin: the Rim Current (Oğuz *et al.*, 1994). The northwestern shelf, see Figure 1, occupies about 20% of the surface of the basin. This

coastal ocean interacts across the shelfbreak with the deep basin circulation. The northwestern shelf region is relatively shallow and there is a region of fresh water influence (Hill, 1998) near the coast, where 80% of the river outflows into the basin occur. The circulation in the interior zone of the northwestern shelf is mostly wind driven (Blatov *et al.*, 1984) and it is populated with weak eddies. The deep basin is bordered, other than to the west, by narrow shelves interrupted with canyons and extended submarine ridges. The interactions between the deep and shelf circulations are complex, strong and intermittent. Internal dynamics, stratification, and topographic variability (slope, orientation, and roughness) lead to the characteristic structure and scales of the Rim Current, the shelf circulation, and their interactions along the periphery. Regional observational programs and, more recently, basin-wide surveys complemented with remotely sensed data (sea-surface temperature (SST), height (SSH) and color (SSC)) have been used to describe the basin variability at different temporal and spatial scales. The observational evidence indicates that the circulation in the basin has a significant mesoscale variability ($O(10)$ km and $O(1-3)$ days). The mesoscale variability is not easily accessible to observations; for instance, the basin-wide surveys HydroBlack91 and CoMSBlack92 were completed by several ships in about one month with about 30 km horizontal resolution. One of the objectives of this paper is to complement these descriptions with dynamically consistent four-dimensional fields of the basin circulation at mesoscale resolution. These fields are obtained with primitive equation model simulations and initialized with basin-wide observations. In this study we employ CoMSBlack92, since it provided the best coverage presently available from basin-wide surveys. A comprehensive description of the *in situ* observations and remotely sensed observations for this summer is contained in Oğuz, Ivanov and Beşiktepe (1998), herein referred to as OIB. The summer mesoscale time variability is explored by studying four-dimensional fields produced with primitive equation data-driven simulations of a few weeks duration. These dynamically balanced multiscale fields complement and extend the description of OIB for this period. The specific goal of this study is to gain insight into the multiscale basin, sub-basin and mesoscale circulation; permanent and semi-permanent elements of the circulation, intermittent events and the overall description of the hydrography of the basin during the summer season.

The approach to obtain a representation of the spatial and temporal multiscale variability of the Black Sea circulation is to dynamically evolve the basin-wide, quasi-synoptic datasets of CoMSBlack92. The data gridded, via optimal interpolation, to an eddy resolving grid are used to obtain initial conditions for an eddy-resolving rigid lid primitive equation model. Simulations for the season, forced by wind stress and riverine inflows are used to obtain typical summer evolutions as represented by simulation for the summer-autumn of 1992.

In addition to the scientific interest in understanding the Black Sea biological, chemical and physical processes and interactions, there are compelling practical motivations (Mee, 1992). Drastic changes have occurred in the Black Sea ecosystem in the last decades. These include bottom hypoxia in the northwestern shelf, large shifts in the marine species

and population, and changes in the nutrient structure with great impact on the fisheries. An integrated system approach for the acquisition of knowledge about the basin, aimed to support scientific and management activities, is the regional multidisciplinary Ocean Observing and Prediction System (OOPS) (Andersen, 1997; Robinson *et al.*, 1999). The OOPS combines physical, biological, and chemical observations with multidisciplinary dynamical models through data assimilation schemes (Robinson *et al.*, 1998), in order to efficiently and adaptively acquire accurate estimates of the present and future states of the system. Tuned physical, biological and chemical dynamical models capable of accurately tracking important processes in the basin are required. In this context, one of the objectives of this paper is to initiate the assessment of the ability of a tuned primitive equation model to represent physical processes which significantly influence the biogeochemical processes in the Black Sea.

Early studies of the Black Sea circulation based upon numerical models were concerned mainly with large spatial scales and seasonal and interannual variations (see for instance Gamsakhurdiya and Sarkisyan (1976)). These initial studies were reconstructions of the velocity fields based upon given estimates of the mass field. It is worth noting that in the course of these studies in the Black Sea, the joint effect of baroclinicity and topography concept was established (Sarkisyan and Ivanov, 1971). Sensitivity studies of prognostic models to atmospheric forcing, lateral forcing, and topography in the seasonal and interannual time scales have been of major interest in modeling (see for instance: Demishev and Korataev (1966); Oğuz *et al.* (1995); Oğuz and Malanotte-Rizzoli (1996); Stanev (1990); Stanev and Beckers (1999b) and references therein). These studies clarified important dependencies on the forcing of the basin and sub-basin scale circulation and the thermohaline structures, including the large-scale estuarine regime of the basin (Caspers, 1957), the formation and spread of cold intermediate waters (Ovchinnikov and Popov, 1987), and the large structure of the circulation. These studies have been complemented with concise descriptions of the large-scale surface circulation seasonal variability using spectral representations with a few degrees of freedom (Eremeev *et al.*, 1992). This study presents simulations of the Black Sea variability at mesoscale resolution over the entire basin during a summer-autumn season, including dynamical (intermittent) events in close relationship to observations, to our knowledge for the first time.

The observational basis of this study consists of the 1992 basin-wide surveys and atmospheric forcing described in Section 2. The data in Section 2 are used in the preparation of initial conditions for a primitive equation model. The dynamical model numerical characteristics open Section 3, followed by a description of the initial fields preparation. Details on the calibration of the data-driven simulation and complementary sensitivity studies to subgrid parameterization, geometry and wind forcing close Section 3. In Section 4 the major circulation elements and events in the simulation are described and compared with observations. In this section we also discuss new information derived from the simulation. Of particular interest are intermittent events found in the observations and in the data-driven simulation: surface jets, squirts, formation and coalescence of eddies,

etc. The closing section summarizes the results and suggests some questions regarding dynamical processes motivated by our results and delineates future work.

2. Data

The Black Sea is a semi-enclosed sea connected to the shallow (10–20 m) Azov Sea through the Kerch Straits and to the Mediterranean Sea through the Bosphorus Strait, the Marmara Sea and the Dardanelles Strait (Fig. 1). The flat abyssal plain (20% of free surface, depth > 2000 m) rises to the continental shelves. The northwestern shelf (mean depth 50 m) has a shelfbreak at about 100 m with the Crimea peninsula to about the latitude of Varna to the south. The Danube fan and the Kerch fan are gentle continental slopes. The other portions of the shelf are narrow (<20 km), fractured by canyons, abrupt ridge extensions and steep continental slopes. A typical slope value is 0.1.

a. Hydrography

The temperature and salinity data used in the present simulation are from the CoMS-Black'92 data set, collected in a collaborative effort by several institutes from the Black Sea countries (Oğuz *et al.*, 1993). The data consist of 313 CTD profiles on an almost regular grid with 30 km spacing. Although the majority of the stations were visited between 7–26 July, the survey was carried out between July 4 and August 2, 1992. The CTD casts sampled the water to a nominal depth of 500 m, except for 16 deep CTD casts (1500 m) used for intercalibration. The intercalibrations were done utilizing deep CTD data from the same station visited by each ship. The pooled data set consists of vertical profiles of temperature, salinity with 1 m vertical resolution at each station. The final data set is accurate to about 0.005°C in temperature and 0.005 ppt in salinity.

A detailed description of this data set, including a kinematical description of the circulation based upon geostrophic velocity estimates and the hydrographic characteristics of the Black Sea, is contained in OIB. Here, we highlight some of the hydrological conditions observed during this cruise. The reader is referred to OIB for further details.

The surface mixed layer has a depth between 15–25 m with a relatively low salinity (17–18.5 ppt). The brackish coastal water has the lowest salinities of about 14 ppt on the western boundary near the rivers with the larger outflows. Salinity of 18 ppt is considered as a boundary between coastal and interior waters during the summer. The surface temperatures vary between 23–27°C. The minimum temperature in the water column occurs in deep waters around 50 m, whereas in the basin boundaries the minimum is generally deeper (100 m). This relatively colder layer, named the Cold Intermediate Layer (CIL), is observed all around the basin. A temperature of 8°C is considered as both an upper and a lower boundary of the CIL. The CIL forms in the northwestern shelf (Blatov *et al.*, 1984) and over the central portion of the basin in winter and spreads over the basin during spring and summer (Ovchinnikov and Popov, 1987). Below the CIL, the main halocline/pycnocline separates the deep waters of the density $\sigma_\theta \sim 17 \text{ kg/m}^3$ from the

shallower upper layer waters of $\sigma_\theta \sim 11 \text{ kg/m}^3$. The temperature and salinity distribution below the pycnocline increases slightly with depth. The pycnocline is also the boundary between oxic and anoxic waters of the Black Sea. We found that in the summer of 1992 the layers with potential density $\sigma_\theta > 14.1 \text{ kg/m}^3$ are partially in contact with the atmosphere. The deep basin main pycnocline $\sigma_\theta[14.2\text{--}16.2]$ intersects the bottom in the range of 35–120 m. Temperature and salinity on isopycnals surfaces with $\sigma_\theta > 14.3$ are nearly homogenized. The geostrophic potential vorticity is also nearly homogenized in the main pycnocline layers.

Rivers discharging into the northwestern shelf include the Danube ($203 \text{ km}^3/\text{year}$), the Dnieper ($54 \text{ km}^3/\text{year}$) and the Dniester ($9.3 \text{ km}^3/\text{year}$) (Andrianova, 1997). These rivers, together with the Rioni River ($10 \text{ km}^3/\text{yr}$) in the east coast, and the Sakarya, Kizilirmak and Yesilirmak rivers along the Anatolian coast, with about $6 \text{ km}^3/\text{year}$ of outflow each, account for 90% of the river runoff. See Figure 1 for locations.

b. Atmospheric forcing

The daily surface wind stress was obtained from the Sevastopol MSIA/URHI wind velocities for the simulation period. These wind velocities were computed from daily maps of sea level atmospheric pressure on a grid 40 to 40 miles and then interpolated to a 20 by 20 miles grid to calculate surface wind field. Figure 2 shows four consecutive days of the wind stress. These patterns are typical for this time of the year. The wind is generally stronger in the western part of the basin and the magnitude of the wind stress can reach up to 5 dyn/cm^2 . Strong wind events occur about every 10 days and last about 3 days. The winds generally are northerly and show a cyclonic tendency. The heat fluxes employed here are as in Oğuz *et al.* (1996). The estimates were based upon previous climatologies, corrected for overall balance. The net heat flux is, on average, about 350 W/m^2 , with temporal variations of about 50 W/m^2 over a month.

3. Model

A useful circulation model for the Black Sea must be capable of resolving dynamics at horizontal scales smaller than the mesoscale eddies and must capture the vertical structure, such as strong relatively shallow stratification over steep topography. Turbulent vertical mixing and diffusivity are important in the shelves and in the highly vertically sheared currents in the slope and shelves. The dynamics are approximated with a numerical model implementing primitive equation dynamics and a parameterization for turbulent vertical mixing and diffusivity. The model is initialized using the hydrographic observations described above. The mapping of temperature and salinity observations to the model grid is carried out using a two-scale objective analysis (Lozano *et al.*, 1996). The initial velocity is approximated with a geostrophic velocity derived from a dynamic height reference to a level of no motion. The dynamic height on the slope and shelves above the level of no motion is estimated by extrapolation of the bottom density. The effort in the preparation of

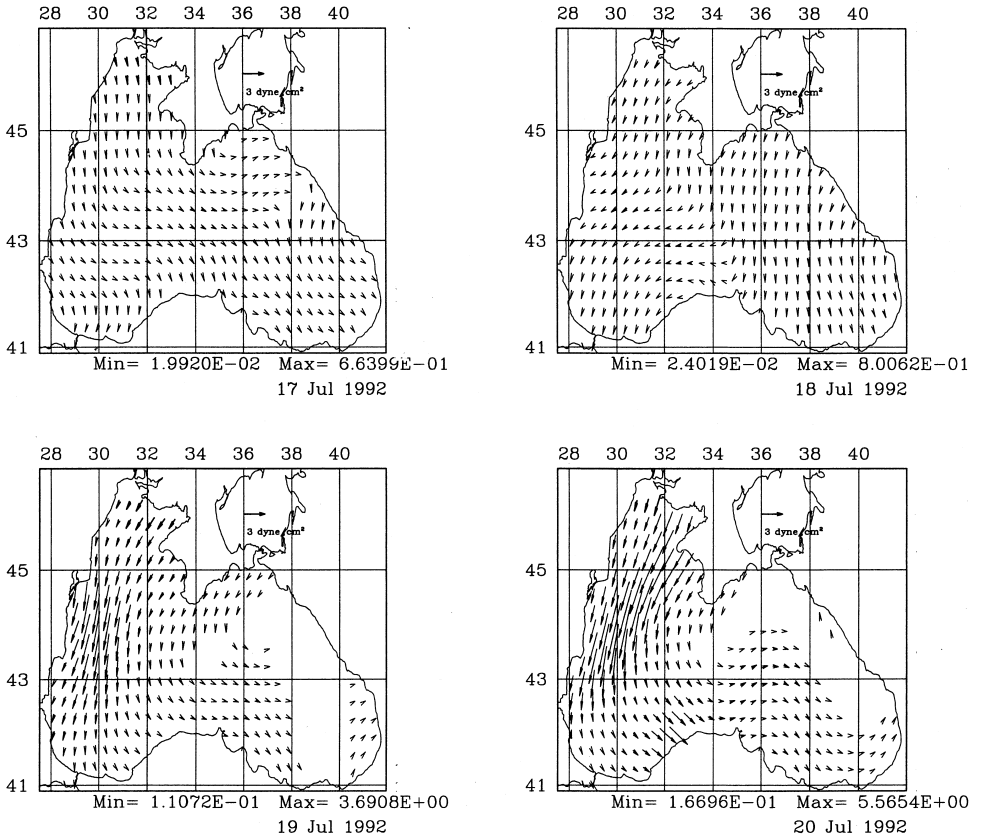


Figure 2. Wind stress for July 17–20 1992, derived from the Sevastopol MSIA/URHI winds.

the initial conditions is directed to shorten the equilibration time of the simulation. The calibration of numerical and physical parameters uses, in part, comparisons with available observations.

a. Dynamical numerical model

The dynamical model employed here is the Primitive Equation Model (PE) of the Harvard Ocean Prediction System (HOPS), (Lozano *et al.*, 1994; Spall and Robinson, 1990). For recent applications of the HOPS and the primitive equation model in other regions of the World Oceans see Robinson *et al.* (1998) and Lermusiaux (1999). The PE numerical model assumes Boussinesq and hydrostatic approximations. For this study we further assume the rigid lid approximation, implemented here in the streamfunction formulation. The selected parameterization for turbulent vertical mixing and diffusion is the Richardson number dependent K parameterization of Pacanowski and Philander (1981). The lateral boundaries are closed except the entrance of the Bosphorus Strait at the

Marmara Sea and the major rivers. At coastal boundaries there are no heat and salt fluxes, and a no slip conditions is set for the momentum equations.

The main numerical attributes of the numerical model are as follows. The state variables (temperature, salinity, transport streamfunction and internal velocity) are defined in the B-grid (Arakawa, 1996) with terrain following coordinates in the vertical. The spatial operators are second order finite differences, except for a cubic spline algorithm employed for the pressure gradient. The discretization of the vertical coordinates is implemented with a double sigma coordinate system (Haley, 1996) designed to maintain nearly flat levels near the main pycnocline and accommodate steep and tall topographic features. The time stepping is the leap frog algorithm with the time filter of Asselin (1972) to control numerical modes. The Coriolis and vertical mixing terms in the momentum equation and vertical diffusivity term in the tracer equations are treated semi-implicitly in time. In the horizontal, the fields are smoothed with a Shapiro (1970) filter. The filter selectively removes small scales while keeping large scales.

b. Objective analysis

In this subsection we discuss the preparation of the initial fields for the dynamical model. The observations are gridded onto the model grids via a two-stage Objective Analysis (OA) scheme (Lozano *et al.*, 1996). A field ψ is estimated by $\psi_E = \bar{\psi}(x) + \psi'$. The first OA is used to estimate the (spatially variable) mean $\bar{\psi}$; the second OA determines the mesoscale ψ' . In the first stage, the large-scale fluctuation $\psi_L(x)$, from a uniform mean ψ_0 is estimated to obtain an estimate of the mean $\bar{\psi}(x) = \psi_0 + \psi_L(x)$. In the second stage of the scheme the mesoscale fluctuation $\psi'(x)$ from the mean $\bar{\psi}(x)$ is estimated. The OA uses the Gauss Markov theorem (Bretherton *et al.*, 1976). The form of the correlation in the two stages of the OA is identical, and varies in the value of the parameters. The correlation C between two events at the points x, y occurring at the times t_x, t_y , respectively, is modeled by

$$C(x, y) = \left(1 - \frac{s^2}{D_2^2}\right) \exp\left[-\frac{s^2}{2D_1^2} - \frac{(t_x - t_y)^2}{\tau^2}\right];$$

where, $s = (x - y)'(x - y)$, prime denotes the transpose of a vector; τ and D_1 are time and space decorrelation scales, respectively; and D_2 is the zero crossing of the correlation function C .

The time and space decorrelation scales used to grid the temperature and salinity fields are listed in Table 1. The selection of these parameters was based upon the following considerations: (i) The scales chosen were driven in part by the coarseness of the sampling. The (multi-ship) basin-wide survey took about one month. The time decorrelation length τ of one month was found to avoid shocks in the evolution of the fields after initialization. The nominal horizontal distance between observation points is about 30 km. The Rossby radius of deformation, as derived from the data set, is 22 km. Expected advective mesoscale has a size of about three Rossby radius of deformation; whereas event

Table 1. Objective analyses scales.

Correlation Scale	Time τ (d)	Crossing D_2 (km)	E -folding D_1 (km)
Large Scale	∞	200	100
Mesoscale Scale	30	60	40

mesoscale commensurates with the Rossby radius of deformation. The latter scale is poorly resolved in the model. The nominal grid resolution is 9 km. (ii) The gridded fields are insensitive to changes of about 10% from the spatial scales listed in Table 1. (iii) Finally, the e -folding mesoscale decorrelation scale agrees well with the estimates derived from a basin-wide 1988 summer dataset (Grigor'ev *et al.*, 1996). In this study, the spatial scales were found to increase somewhat with depth. No attempt was made to include this effect.

In this study, the interest is focused on the ability of the model to represent the dynamical evolution of the sea at mesoscale resolution. The fields in the upper layers produced by the model in a few days after initialization have shorter de-correlation scales than in the initialization fields, as expected. The spatial scale in the simulation is about 20 km, and the temporal scale is about 3 days.

The temperature and salinity observations are mapped to an intermediate grid using objective analyses. The intermediate grid has the same discretization in the horizontal as the PE model grid. In the vertical, the intermediate grid has 26 flat levels at the following depths (in meters): 3, 5, 10, 15, 20, 30, 40, 50, 60, 75, 100, 125, 150, 200, 250, 300, 400, 500, 600, 700, 800, 900, 1000, 1400, 1800 and 2000. Temperature and salinity measurements were carried out nominally down to a depth of 500 m and the 16 stations were made all the way to the bottom. Because of the uniformity of the water mass properties below 500 m and very slow evolution in time, the temperature and salinity profiles obtained during September 1991 were used as a background.

c. Initial fields

The model initialization temperature, salinity and velocity at 10 m are given in Figure 3. The surface temperature (Fig. 3a), varies between 18°C and 26°C in the basin. This initial temperature distribution reveals significant spatial inhomogeneity and signatures of anticyclonic circulation. Large-scale patterns can also be perceived. The most notable pattern is the large-scale temperature zonal gradient increasing to the east. The surface temperature field becomes more organized and coherent in the course of the simulation at large scale and mesoscale, connecting different dynamical structures. The simulated SST more closely resembles AVHRR patterns than the initialization. The partial lack of coherence in the initialization is due in part to the asynopticity and resolution of the data set.

A distinguishing feature of the surface salinity distribution (Fig. 3b) is the presence of an inner shelf front associated with the fresh water inflow from large rivers in the northwest-

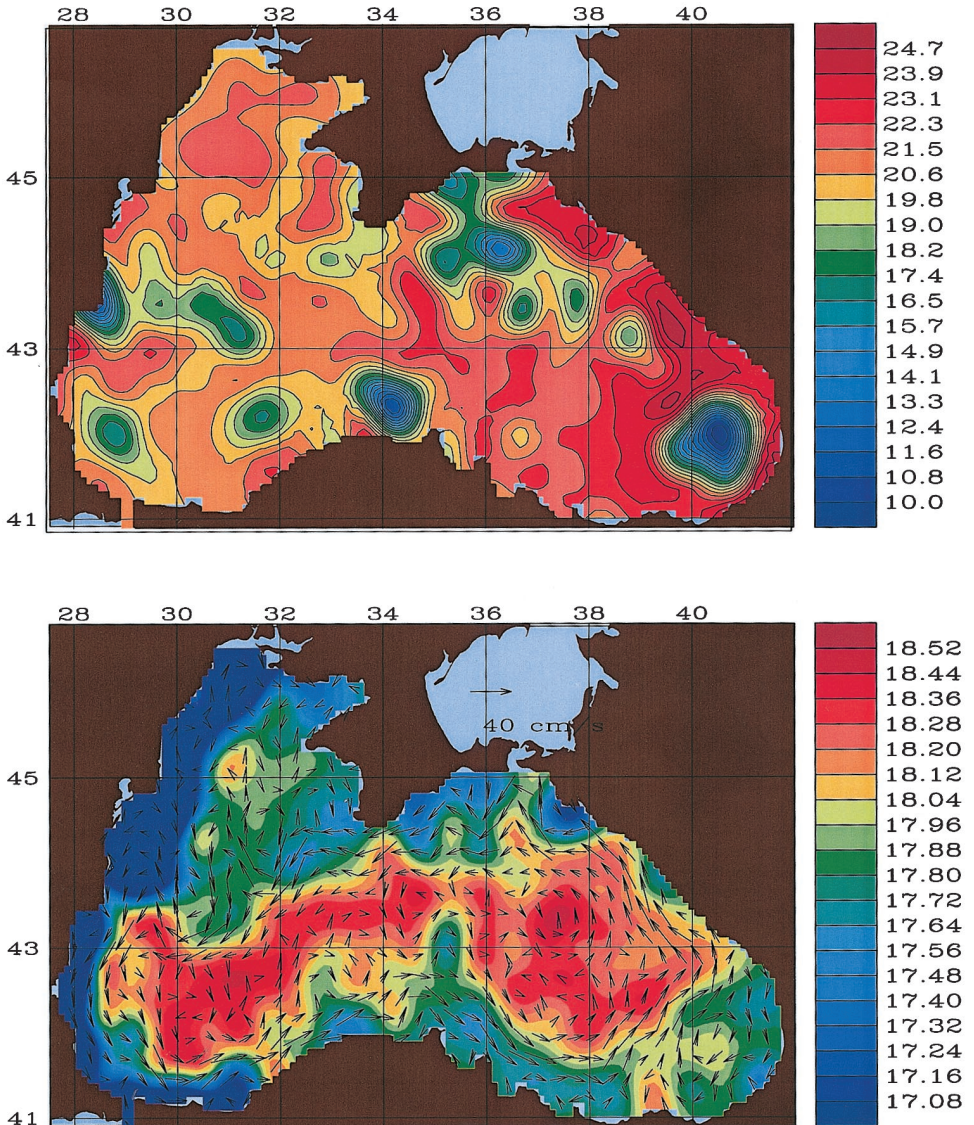


Figure 3. Initial conditions. Temperature (upper panel), salinity and velocity (lower panel) at 10 m.

ern shelf. A salinity of 18 ppt establishes an interface between river-originated coastal waters and the interior waters. The river water is traced down to the Bosphorus entrance region in the form of a narrow coastal strip of current with salinities of 17.4 ppt. As a result, coastal waters have low density and they are observed as a strip all around the basin.

The surface dynamic height (not shown) resembles the hand reconstructed field constructed in OIB by combining data and remotely sensed observations. The resulting

initial surface velocity clearly shows the Rim Current and mesoscale anticyclonic eddies around the basin. Most of the elements of the Black Sea circulation are present in Figure 3; some of them are missing and, in general, the strength of the currents is relatively weak at mesoscale scales. This point will be taken later at the end of Section 4.

d. Initial velocity estimate

The initial velocities are computed assuming a geostrophic balance. Based on observations in the Caucasian (eastern) coast (Titov, 1980), it has been found that a level of no motion at 500 m level is adequate for geostrophic calculations in the deep sea. Because of the uniformity of the water masses below 500 m, geostrophic estimates vary little with a level of no motion in the range of 500–1000 m with the exception of areas with strong baroclinic activity. In our observations, data below 500 m are mostly climatological. In order to evaluate the effect of level of no motion selection in our results, two additional simulations, with 300 m and 1000 m were conducted similar to the central simulation. There were no noticeable differences in the upper levels with respect to the central simulation with 500 m level of no motion.

The central simulation has velocities with a speed of 5 cm/s and 3 cm/s at 500 m and 1000 m, respectively. The velocity patterns at 500 m relate to mesoscale motions in the upper levels whereas at 1000 m there is no apparent correlation with the upper levels.

Based on the results of these sensitivity tests and considering that the survey was designed with most of the CTD casts reaching down to 500 m, we have chosen 500 m as a level of motion in computing model initial velocities. On the slopes and shelves, above the level of no motion, dynamic height was computed using extrapolated values of bottom density. This extension is essential in order to obtain a coherent circulation on the shelves and slope. The geostrophic surface velocity estimated in this fashion has a well defined and narrow Rim Current over the entire periphery of the deep water. This estimate of the geostrophic velocity was further modified in order to ensure no flow across the coastal boundary at the surface. The approach is to construct a streamfunction for the geostrophic surface velocity with a constant value along the coastal boundary. In particular, this ensured that anticyclonic circulation cells near the coast were closed.

e. Model setup, calibration and sensitivity studies

In this subsection some modeling considerations regarding the dynamical evolution of the initialization just described are discussed.

i. Geometry. The model grid covers the entire Black Sea at a resolution of 9 km with 28 levels in the vertical. The horizontal model grid spacing is about half of the radius of deformation in the deep portions of the basin and approximately the radius of deformation in the shallow portions, including the northwestern shelf. A model domain was configured with a finer grid spacing (4.5 km), bottom topography and coastal boundary setup in order to study the effects of increased grid resolution on the simulated fields. Other numerical

parameters and physical parameters in the refined grid model were identical to that of the central simulation. A comparison of the fields derived from the central experiment and those from the finer resolution model, the latter not shown here, during a fifty day period show good agreement (position, strength and phase) in the basin, sub-basin and mesoscale circulation elements. Differences between the two simulations are observed at the smaller scales and also near the coast. The smaller scales in the tracer fields as resolved in the refined grid model simulation show better patterns associated with steering. These comparisons indicate that the structures and patterns of the circulation presented in this paper are supported by the simulations with twice the horizontal grid spacing. In previous simulations with a coarser grid resolution for this basin (see for instance Stanev (1990)) and this study (18 km), important elements of the circulation are either poorly resolved (for instance the Rim Current) or missing (for instance eddy generation).

The IOC bathymetry agrees well with bottom depth measurements conducted during recent hydrographic surveys. The model bathymetry was prepared as follows. The IOC topography datasets consist of digitized isobath contours [IOC, IHO and BODC, 1994 GEBCO Digital Atlas CD-ROM]. Values at isobaths were interpolated to the model grid using cubic splines. The gridded topography is then smoothed, first using a median filter described in Haley (1996) and then using a conditioning procedure to selectively reduced the slope in steep regions (Haley and Lozano, 1999). The purpose of the median filter is to remove small scales supported by three grid points. The reduction of the slope contributes to control errors in the pressure gradient in terrain-following coordinates (Beckmann and Haidvogel, 1993) and improve convergence in the Poisson solver for the streamfunction (Dukowicz *et al.*, 1993). The topography used in the simulations (Fig. 4a) was treated to yield maximum slopes of about 0.05. The conditioning is found to not substantially alter the original bathymetry at this resolution.

The vertical distribution of levels adequately resolves the seasonal thermocline, at about 15 m, and the permanent pycnocline (halocline, between 80 m and 250 m), as well as the bottom boundary layers in the shallow portions of the basin. The level selections were guided to preserve second order accuracy in the vertical (ratios of consecutive vertical thicknesses are kept close to unity) and obtain sufficiently accurate pressure gradient estimates, in particular in the steep continental slopes and near the main halocline (maximum in density vertical gradients). Tests discussed below indicate that 28 levels for the selected topography are adequate. The vertical level distribution is illustrated in Figure 4b. Table 2 summarizes the geometrical parameters used in the model.

In order to ensure that the selected topography and vertical discretization do not support significant spurious pressure gradients, two numerical experiments were conducted. In the first experiment the model is initialized with horizontally uniform temperature and salinity. The vertical profiles of temperature and salinity were selected to approximate the mean profile plus standard deviations in such a manner that static stability was preserved. As expected, the profile departures from the mean were greater in the levels above the bottom of the permanent pycnocline (250 m). The simulation initialized with null velocities

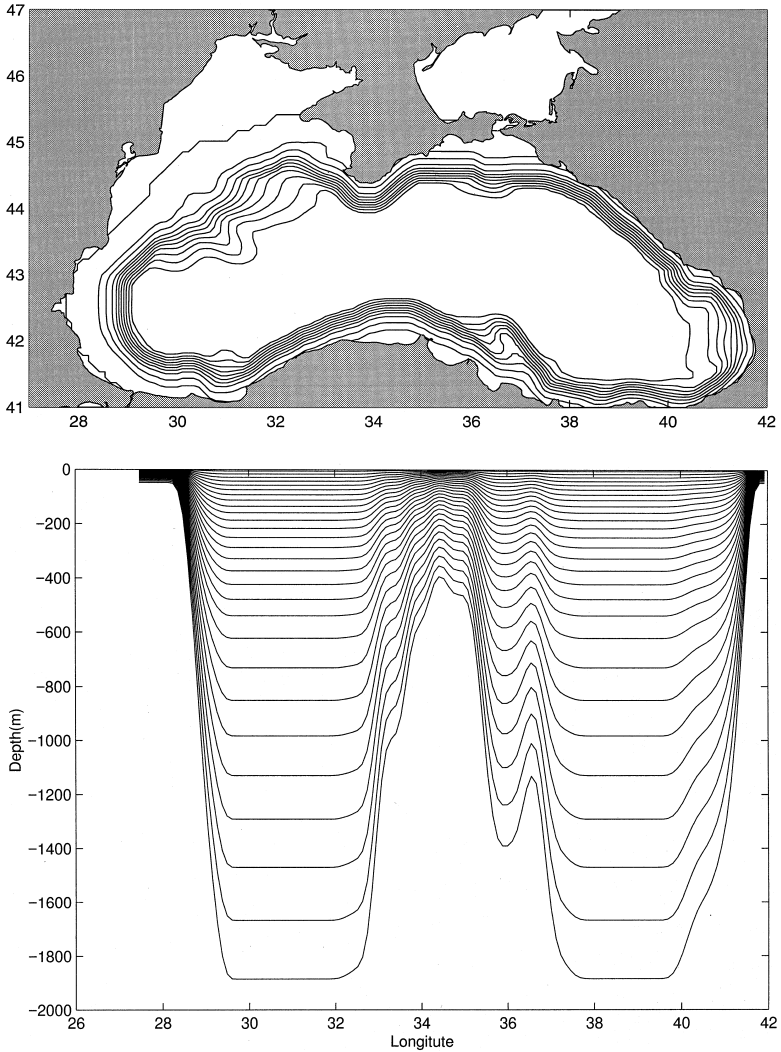


Figure 4. (a) Bottom topography employed in the model. The IOC topography was conditioned for maximum slope of 0.05. Contour intervals in meters 50, 100, and [200:200:1800]. (b) Vertical cross section at 42N, off Anatolian coast, of the model sigma levels at tracer points.

Table 2. Model configuration for the Black Sea

Grid spacing	9 km nominal
Grid size	130 × 74 × 28
Terrain following coordinates	double-sigma
Bottom topography	IOC (smoothed to a slope < 0.05)

generates spurious currents of about 1 cm/s after 2 months. The velocity patterns follow roughly the steep portions of the continental slope. In another set of experiments we employed a topography conditioned to allow steeper slopes, nearly 0.1. The simulations were, overall, comparable to the simulation shown here, but they contained intermittent small-scale noise, especially along rough and steep topographic features and apparently induced by across-isobath flows and associated vertical motion.

The topography for the Black Sea in the ETOPO5 is smoother than the IOC. In the ETOPO5 the steepness of the continental slope, canyons and ridges are poorly resolved. In particular, the slopes south of the Crimea peninsula and the Danube fan and also the Sakarya Canyon and Arkhangelsky Ridge are not well represented. A set of simulations, not shown here, employing these two bathymetries shows substantial differences in the evolution of the fields. In particular, important changes in the circulation can be related to the differences for each of the topographical features referred to above and some are discussed in Section 5 below.

ii. Boundary conditions. The initial fields prepared from basin-wide synoptic data contain the combined effects of atmospheric, lateral forcing and internal dynamics in the basin prior to the synoptic time. In the degree that the initial fields approximate the synoptic conditions, these effects are represented in the simulation. The accurate representation of the incremental effects of atmospheric and lateral forcing after initialization depends, in part, upon the accuracy of the forcing terms. In our simulations, the atmospheric momentum fluxes were derived from analyses with adequate resolution. Other forcings were somewhat simplified, either for their relative importance (Stanev, 1990; Oğuz *et al.*, 1995; Oğuz and Malanotte-Rizzoli, 1996), or the lack of reliable data.

In the central simulation the atmospheric fluxes were set up as follows. Daily wind stresses, derived from the Sevastopol MSIA/URHI winds, were linearly interpolated in time. The net heat flux was set up to be uniform over the basin to an initial value of 350 W/m^2 and varied slowly in time according to climatological values (Oğuz and Malanotte-Rizzoli, 1996). The salinity flux at the surface was maintained at zero. The net heat flux allows the formation of a seasonal pycnocline. The effect of the wind stress on the features of the Black Sea circulation was assessed by running parallel simulations (100 days) with and without wind stress forcing (not shown here). All of the main elements of the circulation exist in both cases except for the strong coastal current on the western boundary of the basin. The strong northerly winds blowing in this part of the basin are conducive to the maintenance of the coastal current. In the absence of wind, river waters disperse and eventually accumulate over the shelf break, and they do not influence the southern coast. The shape of anticyclones are different in the two cases also. With wind, the Sevastopol (44.5N, 32.2E), and Kaliakra (43.5N, 30E) eddies are more elongated. The main difference between the two simulations are found in the circulation of the northwestern shelf and southern coastal current. Most of the other circulation elements have differences in shape and phase.

The Black Sea is a semi-enclosed basin. The only opening to the World Oceans is the narrow and small Bosphorus Strait on the southeastern part. The flow through the strait is a two-layer system importing saline and warmer waters from the Marmara Sea and exporting fresher and colder waters. The transport is approximately $10^4 \text{ m}^3/\text{s}$. The influence of the denser inflow waters on the shelves and slope on the circulation is a subject of research. Here we have chosen a simple model for the incremental effect of the strait; namely, the strait is represented in the model as a straight channel with no net barotropic flow at the open boundary and simple relaxation to initial values for the internal velocity and no fluxes for tracers.

The important sources of riverine fresh water are located on the northwestern and south coasts. The influence of the major rivers (Danube, Dnieper, Dniester, Sakarya, Kizilirmak and Yesilirmak) of the basin are included in the following manner. Observed values of temperature and salinity are nudged in the vertical water column nearest to the river mouth. The nudging relaxation time during equilibration is short in order to obtain observed values in a few days. After this initial stage, the relaxation time is computed based upon the climatological river outflow. There is no exchange of momentum with the rivers. Sensitivity studies with and without rivers showed that including the rivers' outflow improves the representation of the riverine waters near the coast. Outside the coastal regions in the northwestern shelf the simulations with and without rivers differ very little as expected during this season with low riverine outflow. Initial conditions contain accumulated effect of the river outflow and this sensitivity study can only yield the incremental effect during the season. The effects of buoyancy fluxes in the basin can be found in (Oğuz and Malanotte-Rizzoli, 1996).

The boundary conditions at the coastal flow are a no slip condition for the momentum and no normal flux for tracers. The no slip condition is set up by prescribing zero velocity at the boundary and the boundary condition for the Shapiro filter is set to a zero normal gradient at the coastal boundary. The Shapiro filter boundary condition for tracers is similar.

The boundary condition at the bottom specifies no normal fluxes. In the momentum equation the boundary condition is given by the usual bottom stress, with bottom friction coefficient of 0.0025.

iii. Subgrid parameterization. The adjustable parameters related to the effects of turbulence include the horizontal Shapiro filter, the vertical eddy coefficient and the bottom friction coefficient. The values used in all the model runs are listed in Table 3. These values were found to give the best model results for currents and property distributions through sensitivity studies described below.

A Shapiro filter acting on a sigma-coordinate is used to filter the internal velocities and tracers, the latter after removing the initial tracer fields. The parameters (p , q , r) are the order of filter (p), the number of applications of the filter (q), and the filter frequency (r). The filter is scale sensitive and so removes the small scales while keeping large scales. The

Table 3. Model subgrid parameters

Horizontal diffusion	Shapiro filter
Vertical mixing and diffusivity	(4,1,1) velocity (8,1,10) tracers (Pacanowski and Philander, 1981) $\kappa_v = .05 \text{ cm}^2/\text{s}$ (background) At unstable columns $\kappa_v = 100 \text{ cm}^2/\text{s}$
Vertical viscosity coefficient	0.1 cm^2/s
Bottom friction coefficient	0.0025

target was to remove small scales, three grid wave, while preserving the energy-containing scales of the mesoscale. The radius of deformation itself is not well resolved, about two grid spacings; but the mesoscale evolution scales, about three or four radii of deformation, are well resolved. The objective of the sensitivity study for lateral parameterization was to select filters for the velocity and tracers such that the mesoscale evolution scales are resolved, and at the same time avoid small-scale noise. The filters selected for the momentum and tracers implied time decays of 0.3 and 9.0 days for the three grid waves, respectively; whereas scales larger than three radii of deformation are essentially untouched by the filter. The model response to the variation of filter parameters is relatively robust within a reasonable range. If the filters are further weakened, small-scale structures tend to appear and changes in the circulation are small; whereas stronger filters tend to broaden and change the features of the circulation.

The Richardson number dependent formulation of Pacanowski and Philander (1981) was used to formulate the vertical eddy viscosity and diffusivity. Several sensitivity studies were carried out. The choices included a simple constant coefficient in the vertical, and a range of values in the parameters of the Pacanowski and Philander formulation close to the diffusivity estimates from measurements performed during summer 1992 in the Black Sea (Eremeev and Kushnir, 1996). The objective of the sensitivity study was to enable the model to maintain, within observations, the depth of the isopycnals and the distributions of the temperature and salinity along the isopycnals throughout the course of the model simulations. The values in Table 3 coincide with field estimates (Eremeev and Kushnir, 1996) and they were found satisfactory.

4. Summer variability

The discussion of summer variability in this section is based upon the calibrated data-driven simulation initialized with the basin-wide summer of 1992 survey and forced with the observed wind stresses, climatological net heat fluxes and riverine inflows. The model simulation is conducted nominally for the period July 15–September 15, 1992, in the sense that the initialization correspond to the central day of the cruise and the momentum fluxes used are for this time period. The presentation is centered between day 20 and day 45 of the simulation. This period occurs after initial adjustment of the fields and it is representative of the features encountered during the simulation. During the first 15

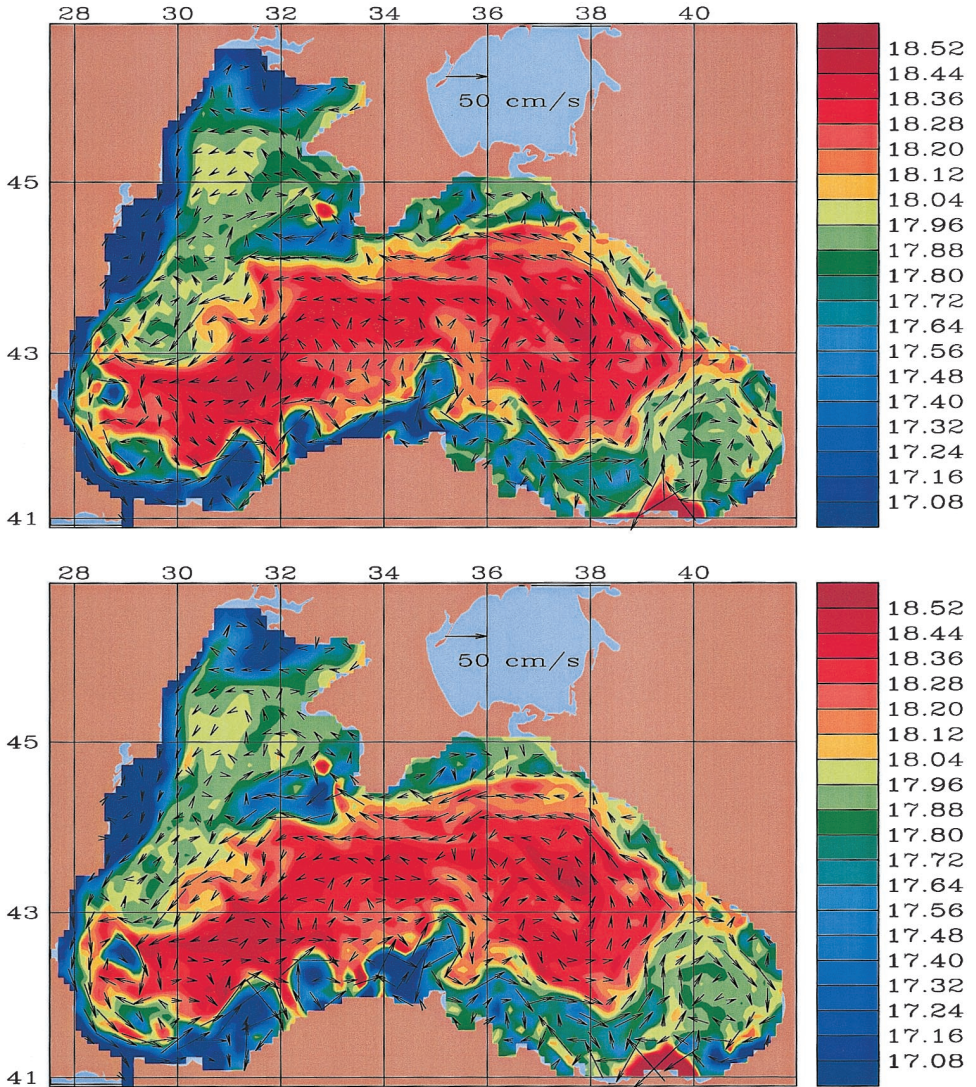


Figure 5. Salinity (ppt) and velocity at 10 m. Day (a) 20, 25, (b) 30, 35, (c) 40, 45. Vector scale as shown in the figure.

days the fields gradually acquire small scales missing at initialization and circulation features become tighter and generally more coherent. To see this effect, compare the fields in Figure 3 with those in Figure 5. At day 10 one of the strongest wind events occurred. Two days later, day 12, visual evidence of this event remains only in the northwestern shelf region, as expected.

The large, sub-basin and mesoscale surface circulation features observed through the

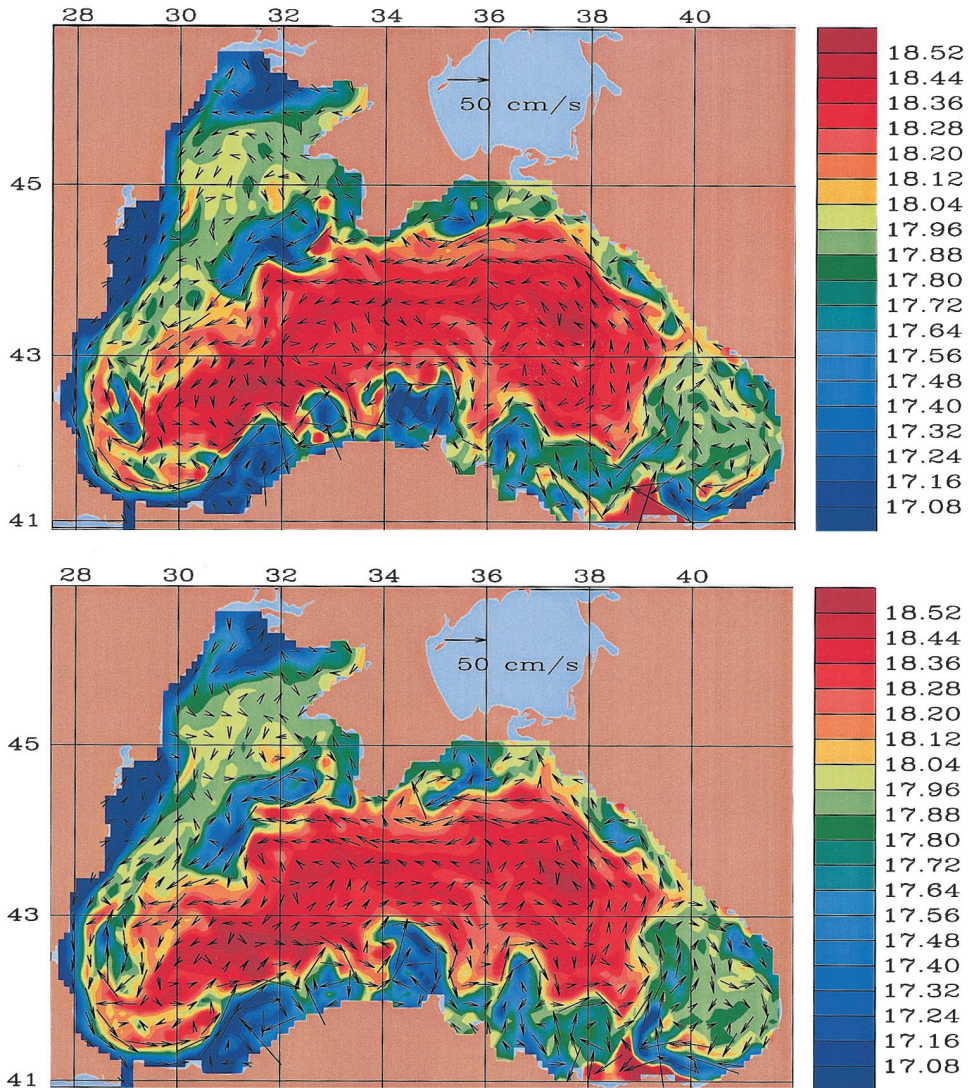


Figure 5. (Continued)

simulation agree in general with historical observations and characteristic elements of the general circulation summarized in the Introduction. In this section a somewhat detailed description of the variability and some physical processes of interest during this period are presented. Comparisons with observations during this period and not used in the simulations and historical observations are also provided. Near-surface fields are first described in order to identify regions, circulation features and regimes. The phenomenological details in specific regions are then discussed using vertical profiles.

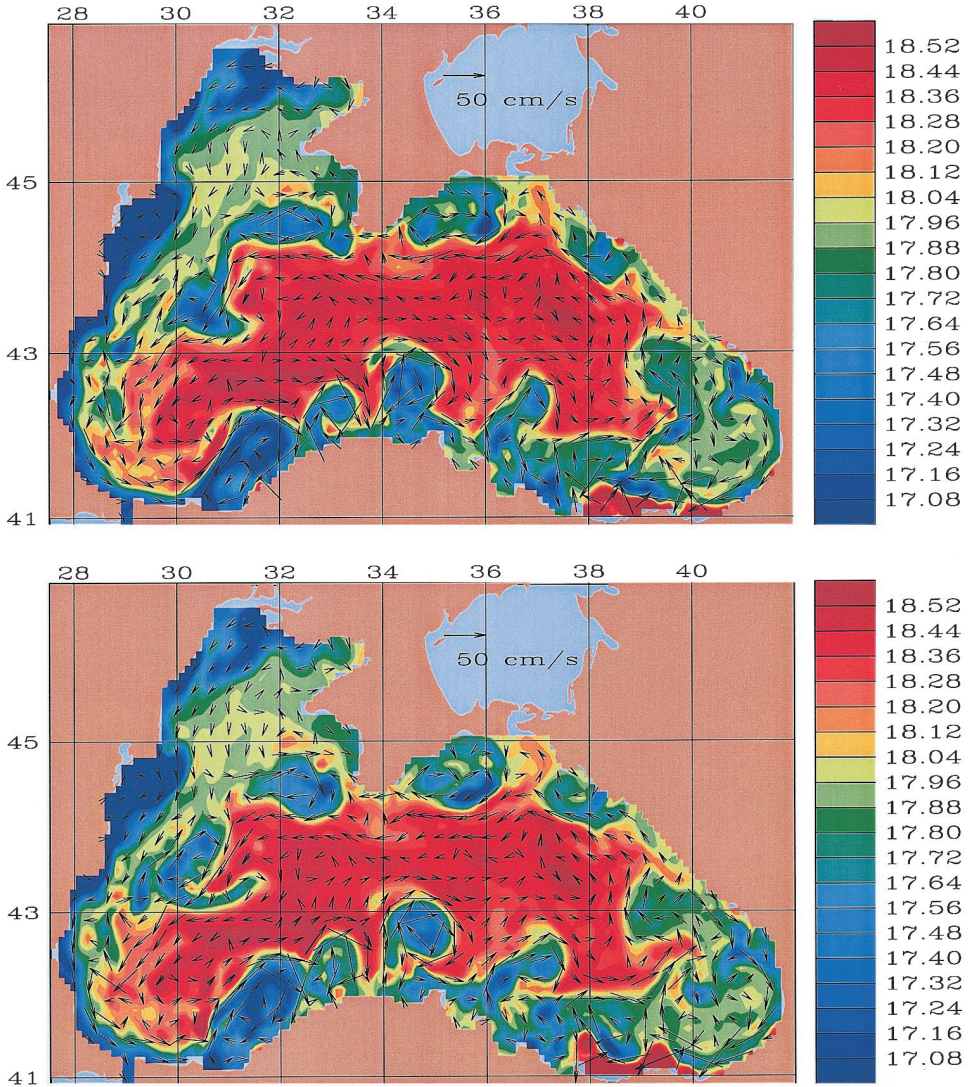


Figure 5. (Continued)

The permanent pycnocline in the deep portion of the sea is also a halocline. The depth of this pycnocline ranges approximately between 80–200 m and has a strong stratification (buoyancy period 7 m). Its formation and maintenance relates to the hydrological balance of this semi-enclosed basin with nearly null water fluxes at the surface, riverine inflows compensated with outflows of relatively fresh waters and inflows of salty and relatively warm waters in the Bosphorus Strait (Ünlüata *et al.*, 1990). In the simulation, the surface water flux is null, major riverine salt and heat fluxes are included and exchanges in the

Bosphorus Strait are kept constant at climatological values. In passing, it is noted that theories advanced to explain the maintenance of the main pycnocline are not conclusive. Above the main pycnocline, cold intermediate waters convectively replenished in winter are capped during this summer by a 10–20 m deep seasonal thermocline. Below the main pycnocline, properties are nearly uniform on density surfaces except in areas with strong mesoscale variability. Below 1000 m flows are sluggish, 1–2 cm/s rms, and with a low correlation with flows in the main pycnocline.

a. Upper layer circulation

The time series (Fig. 5) of salinity and velocity is for a depth of 10 m, every 5 days between days 20 and 45. The time lapse between frames was found to be adequate to see the evolution of features in the circulation. As in OIB, we found that the salinity field is a good tracer for structures at the surface. The large-scale upper layer circulation is characterized by a cyclonic circulation in the center of the basin, intensified over the continental slope around the basin. The circulation in the center region consists of weak cyclonic eddies (≈ 150 – 200 km diameter) interspersed with smaller and weaker anticyclones (≈ 50 – 100 km diameter). In the periphery of the central cyclonic region and over the continental slope is a strong inertial current, the Rim Current. The Rim Current has a speed of ≈ 35 – 50 cm/s at the axis, a width of ≈ 50 km, and a Rossby number ≈ 0.05 – 0.3 , the latter associated to events. The Rim Current axis is roughly traceable by the 18 ppt isohaline in the periphery of the deep basin. The Rim Current is associated with the main pycnocline, usually offshore of the 100 m isobath and it does have strong interactions with topographic structures, anticyclonic eddies at its shoreward side and coastal and shelf waters. A series of anticyclonic eddies along the coastal side of the Rim Current evolve with and interact with the Rim Current and the coastal and the shelf waters all around the basin. The largest anticyclonic gyre, the Batumi gyre, lies east of 38E.

Observations (for instance Blatov *et al.* (1984); Sur and Ilyin (1997); Ginsburg *et al.* (1999)) and the model simulation show that there are distinct structural characteristics and dynamical regimes in different segments of the Rim Current. For presentation purposes we associate different names to some segments of the Rim Current: the Northwestern Shelfbreak Current (NSC), the Anatolian Current (AC) and the Caucasian-Kerch Current (CKC).

Northwest Shelfbreak Current (NSC). This segment originates at the south of the Crimea peninsula and terminates north of the Bosphorus Strait, where it often joins the coastal currents approaching from the north. The main deep basin pycnocline associated to the halocline front intersects the slope at about 100 m. The NSC has large and relatively long meanders. There are two semi-permanent anticyclonic eddy complexes (one or more anticyclonic cores) interacting with the NSC at the northern (Sevastopol eddy) and southern (Kaliakra eddy) ends. During this period, relatively fresher waters around the Sevastopol eddy spread to the southwest, follow the right flank of the NSC, break into cells

and are partially entrained into the deep portion of the basin. The latter phenomenon is related to wind events, and it is a mechanism of exchange between the shelf and deep waters. Another mechanism of exchange, noted in the simulations, is the intermittent deep water intrusions onto the shelf near the bottom. The Bosphorus eddy, often observed to the northwest of the Bosphorus Strait (Oğuz *et al.*, 1992), was not present in the data and in the simulation.

Anatolian Current (AC). Along the Anatolian coast from Bosphorus to the east of the Arkhangelsky Ridge, just before separation from the coastal area, the Rim Current transverses the periphery of a series of anticyclonic cells which dominate the circulation on the shoreward side of the current. In the Anatolian coast, the near-coastal circulation is populated at any given time with three to five anticyclonic cells in close proximity to the coast, with different strengths.

Around the relatively weak anticyclones, a slope current (AC) is well developed. Interactions with the relatively stronger anticyclonic cells divert the slope currents to form the rim of the anticyclonic cells. Further strength and evolution of the anticyclonic cells divert the slope currents toward the offshore, occasionally forming squirts. The AC becomes narrower and reaches to maximum speed (up to 70 cm/s) along the western Anatolian coast. Near Sakarya Canyon anticyclonic eddies form about every 20 days growing to about 40–50 km and moving east with a speed of 15 km/day. The movement of this eddy to the east undulates the Rim Current leading to a meandering jet between 31E and 33E after the Sakarya Canyon. In the portion of the slope not influenced by the anticyclonic activity on the shelves, the current tends to re-establish along the isobaths. Around day 45 an anticyclone is shed into the deep basin near Sinop. We look closely at this event below.

The AC current departs from the isobaths as it passes by the Arkhangelsky Ridge. Downstream from the ridge, the current separates and forms, in the open sea, the rim of the Batumi eddy. The circulation in the eastern Anatolian is complex. There are several eddies, and squirts and filaments are formed intermittently. The river water's salinity helps to view, in part, some of the development of these features. The injection of the low salinity water is visible in the salinity field distribution.

Caucasian-Kerch Current (CKC). Farther downstream, after crossing the open sea around the edge of the Batumi gyre, the current attaches to the Caucasian slope, leading to the formation of the Caucasian-Kerch Current between Sukhumi and the Crimea peninsula. The CKC is found, in general, to be stable following the isobaths. After passing the Novorossiysk, the CKC turns west around an inshore semi-permanent anticyclonic eddy. After transversing the Kerch shelfbreak, the CKC bears again around an anticyclone at the east of Crimea peninsula. This anticyclone gains in strength during the course of the simulation.

Northwestern shelf. The interior of the northwestern shelf circulation is mainly wind driven. Shoreward Ekman flows driven by strong northerlies induce a southward coastal current that carries the river waters south. The strong northerlies also have strong effects on the Sevastopol and Kaliakra eddies. These eddies display elongated structure over the shelf break while their centers do not change position significantly. Southeast of the Kaliakra eddy, there is a highly variable O (1 day) complex of cyclonic and anticyclonic eddies. South of Varna, where the wide shelf break narrows and the NSC approaches the coast, the two currents merge and interact. Often, and intermittently, an anticyclonic eddy forms in the area where these two currents interact and the eddy draws the low salinity coastal waters offshore.

The current in the northwestern shelf region is very weak if the winds are weak. However, when the northerly winds grow in magnitude, which is the dominant regime during summer, a current comparable in magnitude to the Rim Current is generated. The winds also create a strong coastal current which flows very close to the coast and carries the river waters to the south.

Drifters are employed to visualize the circulation during the simulation. Drifter trajectories at given pressure surfaces are shown in Figure 6. The drifters were released at day 7, in different locations of the basin. At each location six drifters were released in a triangular configuration, at 5 db (Fig. 6a) and similarly at 50 db (Fig. 6b) pressure levels. The initial locations of the drifters were chosen to visualize different types of processes occurring in the basin. The initial positions of the drifters are marked with a star sign, and the tick marks occur every 2 days. All of the drifters released at 5 db in the northwestern shelf were transported by the Ekman flow to the Danube mouth. Afterward, they moved slowly toward the south with the riverine waters close to the coast. The ultimate fate of the drifter is not dependent upon its released location, provided it is not influenced by the NSC. The residence time of the particles at the surface waters of the northwestern shelf region is estimated to be about a month. The drifters released at 50 db, which are actually at the bottom of the shelf in the model, slowly drifted to the south and remained on the shelf. The drifters released south of the Crimea peninsula moved with the NSC to the south except for one drifter trapped in the shelf waters of the Crimea peninsula. The drifters moving south reveal a well defined meander with 150 km wavelength and 60 km amplitude. The deeper drifters were captured in the Kaliakra eddy.

The drifters released in the vicinity of Varna and the Bosphorus Strait traveled with the AC along the Anatolian coast. Some of them follow the meandering of the AC, some move offshore in areas where squirts are often observed (Sur and Ilyin, 1997). The wavelength of the meander along the Anatolian coast is about 100 km. The drifters released in deep waters north of the Sakarya Canyon, on the surface, follow a cyclonic circulation, and one of them joins the AC before returning to deep waters. The anticyclonic eddy is clearly visible in the trajectories off the Sinop. Some of the drifters released in the Batumi region are trapped near the coast while two of them remain in the vortex. The drifters released at

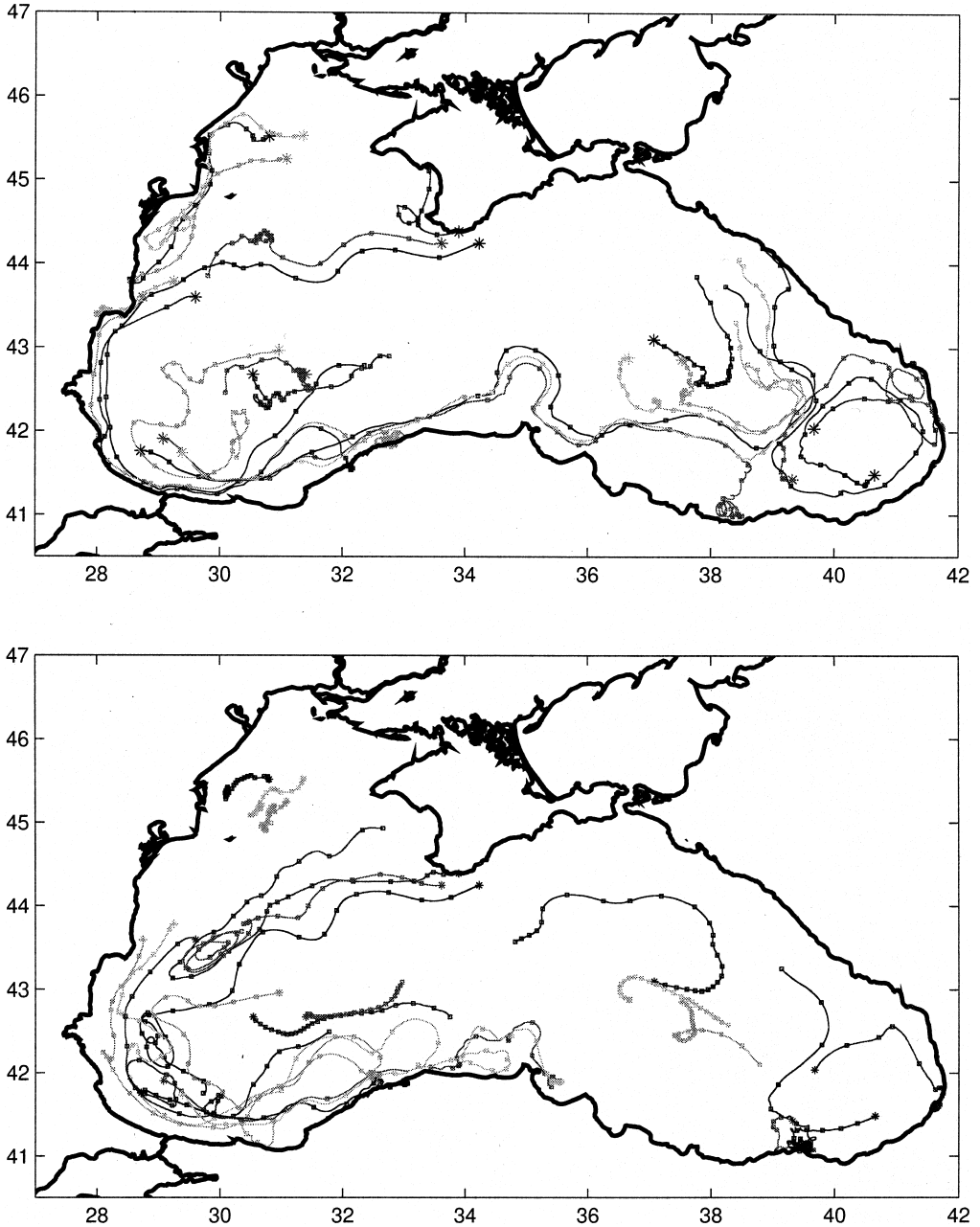


Figure 6. Drifter trajectories along the (a) 5 db and (b) 50 db pressure surfaces. The drifters are released at day 7, the initial locations are denoted by *. Thereafter their positions at every two days are marked.

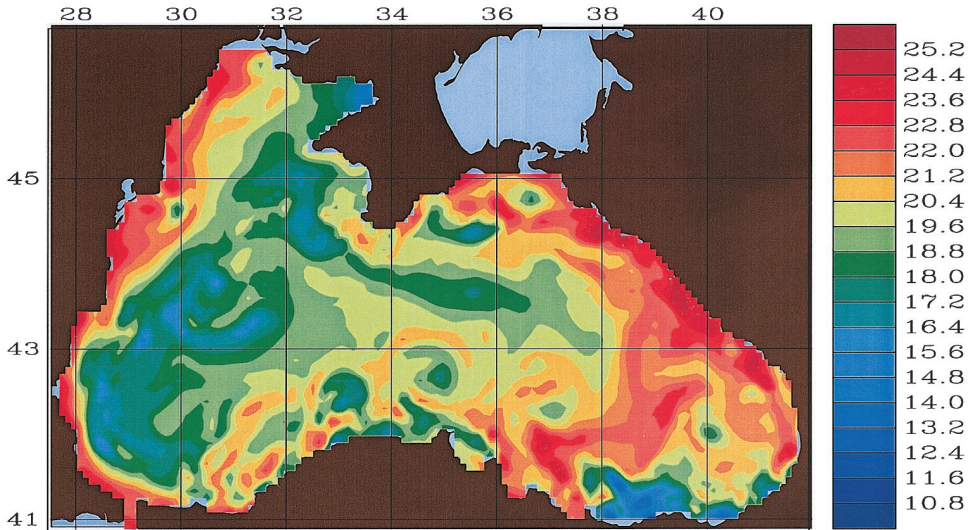


Figure 7. Temperature at 10 m for day 45.

the centers of the eastern and western parts of the basin at 5 db and some of the drifters at 50 db show the generally sluggish cyclonic motion.

i. Sea-surface temperature. The temperature at 10 m shown in Figure 7 corresponds to day 45. Contrast this view with the initialization in Figure 3. The highest temperatures are in the east reaching 26°C . The coldest patches of waters are centered at the centers of the anticyclones over the northwestern shelfbreak and the southwestern coast. The temperature distribution at the surface correlates to the strength of the wind. The large-scale pattern of the surface temperature field reflects the difference of the wind stress at large scales. The stronger winds in the western part of the basin mixes the cold subsurface waters and creates an east-west sea-surface temperature gradient. The centers of the anticyclones are generally cooler than their surroundings and it is often possible to identify the eddies with their temperature signature. An exception is the Batumi eddy. The size and shape of the Batumi eddy could not be identified from its temperature characteristics. This is due to the summer time heating and the weakness of the vertical mixing due to the relatively weak winds in this part of the basin. A clear signature of this eddy in the AVHRR is seldom retrieved.

b. Regional phenomena

In general, the simulation presented in the previous section shows good agreement with the historical data and the structure and strength of the surface features agree well with satellite observations. In order to show the processes observed in the simulations and to compare with observations, we will focus on different parts of the basin in the following subsections.

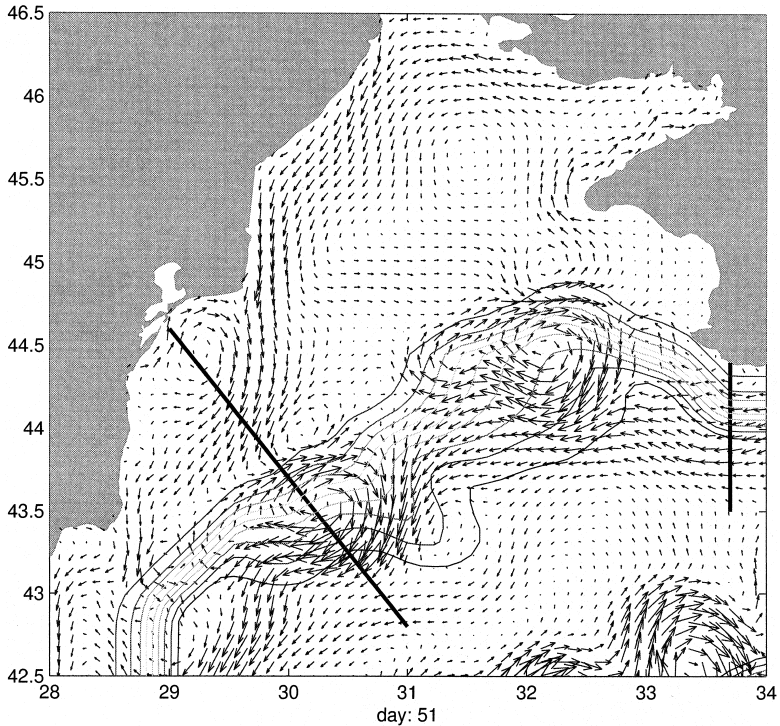


Figure 8. Northwestern shelf region. (a) Surface velocity at day 51, the contour lines trace the model continental slope. (b) Vertical section along track shown in (a) south of the Crimean peninsula at day 51. Normal velocity (cm/s) (upper panel) and $\sigma\text{-}t$ (kg/m^3). The normal velocity pointing into the paper is positive. (c) As in (b) but for the track off the Danube Delta through the Kaliakra eddy.

i. Circulation in the northwestern region. The surface velocity in the northwestern region of the basin is given in Figure 8a. The mesoscale structures are two anticyclonic eddies (Sevastopol and Kaliakra eddies) over the shelfbreak and the meandering of the NSC in this part of the basin. The Sevastopol eddy has two centers until mid-August, then merges into a single larger eddy afterward through September. The center of the Sevastopol eddy is at 44.5N, 32.2E, and the diameter is 70 km during late August and September.

The Kaliakra eddy is located at the southern end of the wide shelf region and is approximately centered at 43.5N and 30E with 60 km diameter. The Kaliakra eddy moves slightly to the southwest through the simulation period and becomes closer to the coast. A strong coastal boundary current driven by wind and buoyancy interacts and distorts the Kaliakra eddy circulation during strong winds.

Sur and Ilyin (1997) analyzed AVHRR images in the Black Sea to characterize these eddies during summer of 1992. In their analysis, the Sevastopol eddy has two cores during summer and merges into one eddy centered at 44.5–44.6N and 32.1–32.2E with 65 km

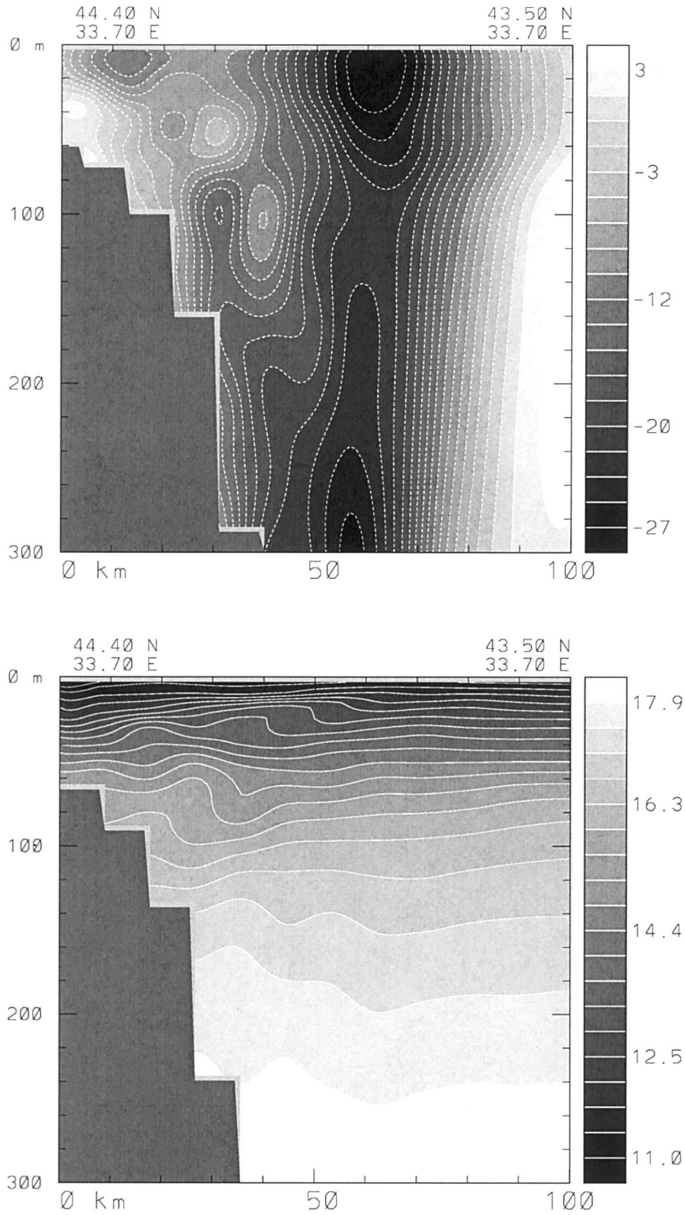


Figure 8. (Continued)

diameter during September 1992. The Kaliakra eddy was located at 43.6N and 30.1E with 60 km diameter (see Table 1 in Sur and Ilyin (1997)). The observed structures of these two anticyclonic eddies, their scales and location fit quite well with the model prediction described above.

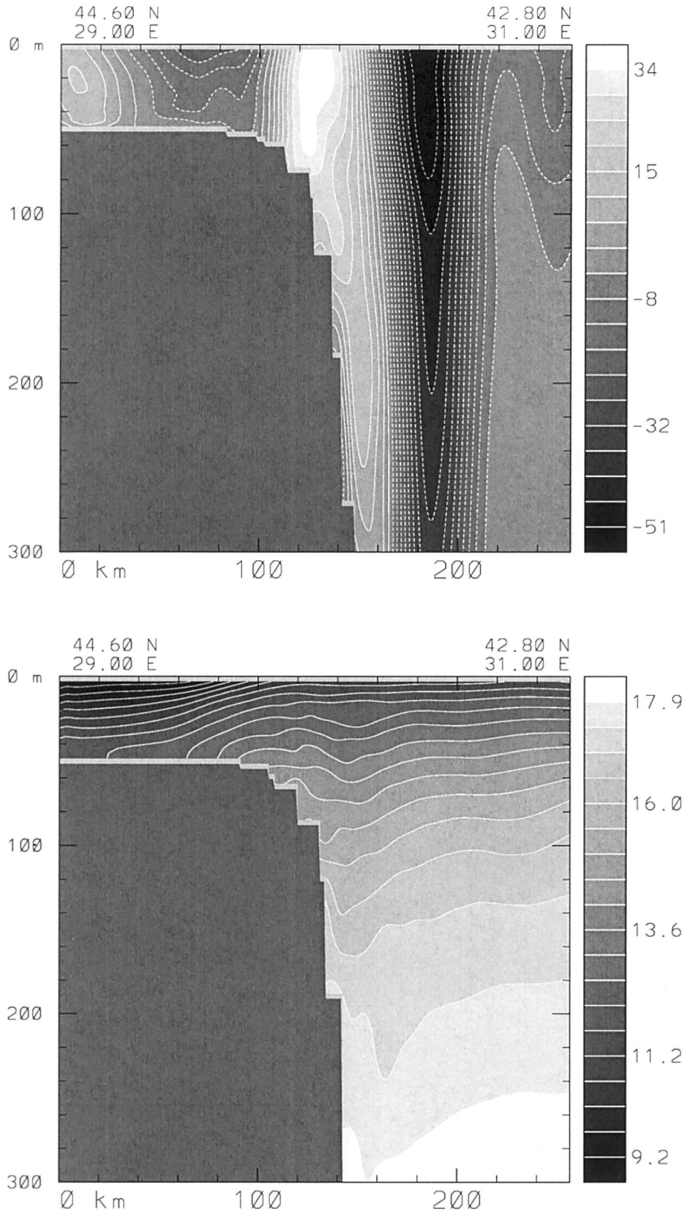


Figure 8. (Continued)

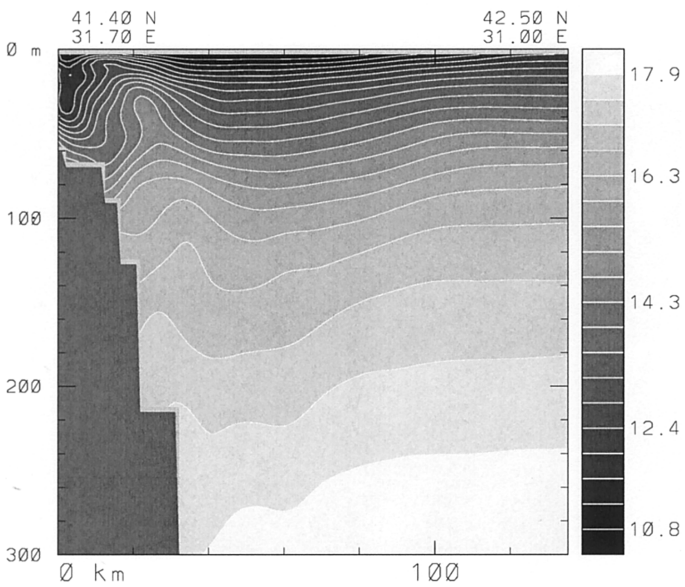
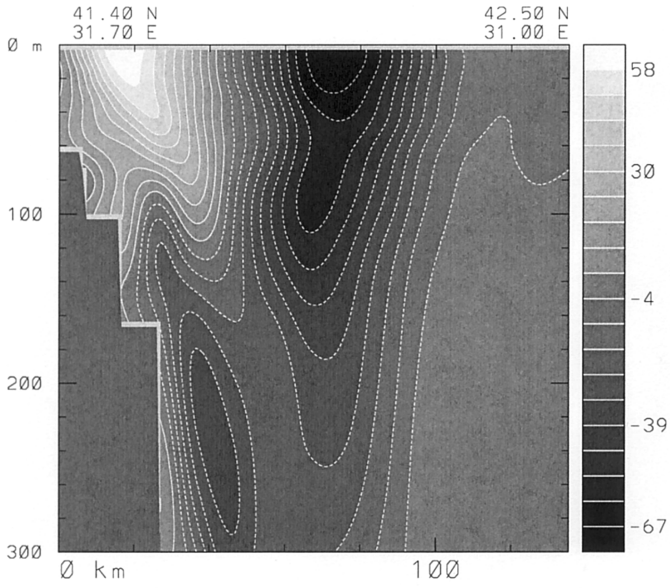
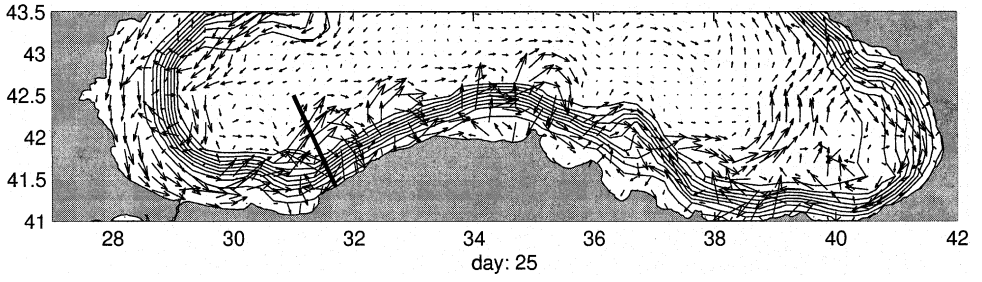
The shelf circulation is characterized by a cyclonic boundary current moving along the coastal boundary. This current accelerates near the Danube, and as it flows southward, it separates at approximately 45.9N after crossing a cape. The current re-attaches to the coast at approximately 43.5N. Between these latitudes an anticyclonic eddy forms on the shore

side of the current. The mechanism of separation seems to be that studied by Klinger (1994); whereby the Coriolis force directed toward the coast is overcome by the centrifugal force as the density current bends along the cape, and an upwelling on the shoreward side develops. There is also a secondary eddy circulation associated to the uplifting on the shoreward side of the density current.

The Rim Current narrows before entering south of the Crimea peninsula, the northwest corner of the basin. As it flows southwestward on the continental slope, the Rim Current encounters diverging isobaths and it bifurcates, with the main branch flowing to the south, and the other turning north and then joining the Sevastopol anticyclonic eddy. The divergence of the isobaths could lead to the bifurcation of the flow in this region (Shi and Chao, 1994). The vertical cross section of density and the normal velocity to the track shown in Figure 8a at the south of the Crimea peninsula shown in Figure 8b corresponds to day 51. The Rim Current entering this part of the basin was 50 km wide and penetrating down to 500 m with a multiple core structure. Speeds of 25 cm/s at 250 m are supported by the disposition of the density surfaces (lower panel). The direct current measurements during Autumn 1993 along this section confirmed the existence of the multi-core velocity structure. The velocities in the simulation compare well with observations (Bulgakov and Kushnir, 1995). However, the simulation did not support the deep counterflow underneath the NSC as reported by these authors. However, existence of the deep counterflow in the Black Sea is not proven yet by other observations and modeling studies (Stanev and Beckers, 1999b). Overall in the slope, and below the seasonal thermocline, the simulated vertical structure of the current is mostly coherent in direction and diminishes with depth. The volume transport of the Rim Current passing through this section in the upper 300 m is computed to be 2.2 Sv.

The transect in Figure 8c of the velocity and density of the eddies on the track shown in Figure 8a over shelf and shelfbreak from the Danube mouth is also for day 51. The Kaliakra eddy was then about 75 km wide, with a maximum core speed of 50 cm/s. The eddy is confined to the upper continental slope, close to the shelfbreak. The eddy can also be seen in the density transect as v-shaped isopycnals. On the onshore side of the section, the river influence can be seen as a low density pool over the shelf. The anticyclonic eddy to the south of the Danube River is also seen over the shelf extending over the entire water column.

Figure 9. Anatolian region. (a) Surface velocity at day 21; the contour lines trace the model continental slope. (b) Vertical section along track shown in (a) from the Baba Point across the Sakarya Canyon at day 25. Normal velocity (cm/s) (upper panel) and $\sigma-t$ (kg/m^3) (lower panel). The normal velocity pointing into the paper is positive. (c) Surface velocity in the central Anatolian region shows the generation of an anticyclonic eddy near Sinop around day 21 (upper panel) and its subsequent detachment (lower panel). The contour lines trace the model continental slope. (d) Dynamic height (0/500 db) derived from four consecutive surveys in the summer of 1984. I June, II July, III August, IV September. (Reproduced from Latun (1990).)



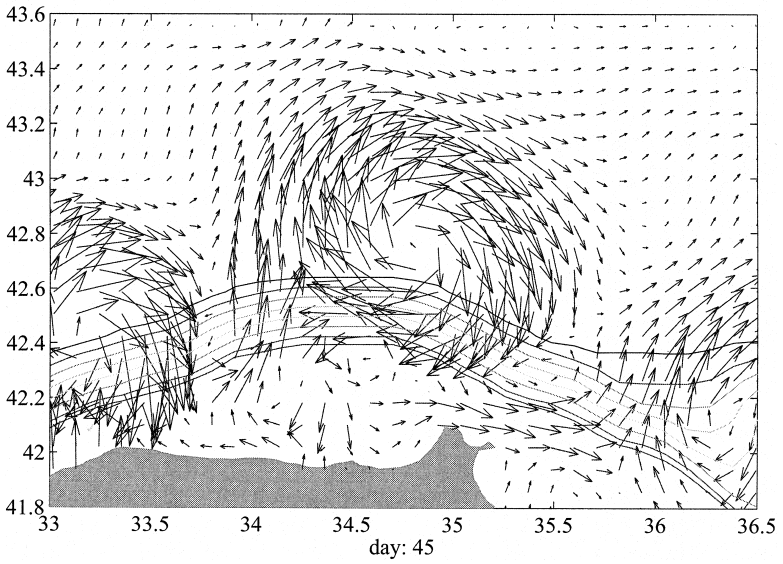
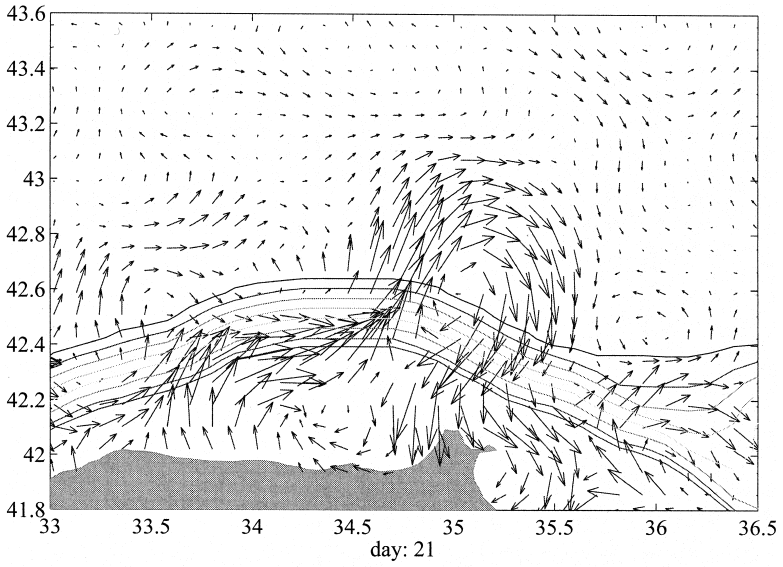


Figure 9(c). Continued

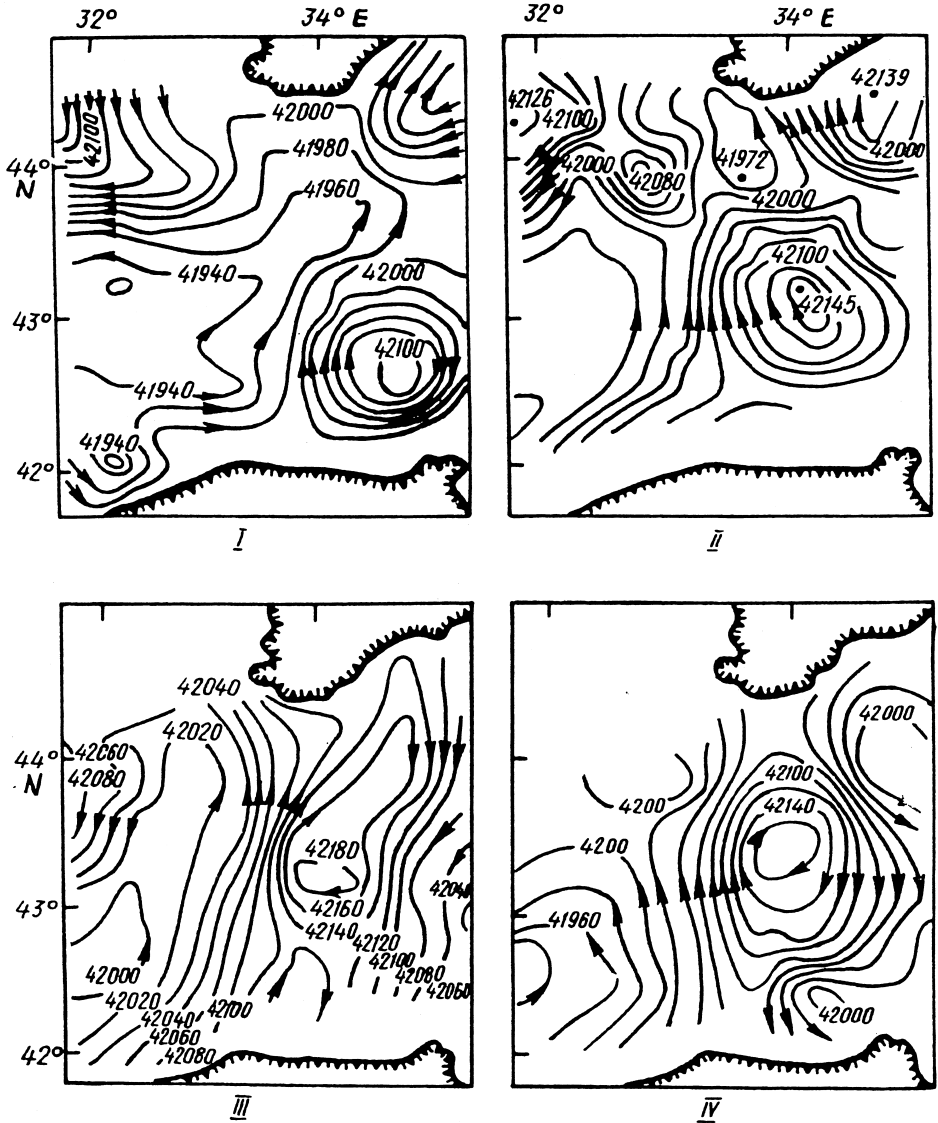


Figure 9(d). (Continued)

ii. *Anatolian Current*. The velocity at day 25 of the model simulation along the Anatolian coast is shown in Figure 9a. The core speed fluctuates in the 30–50 cm/s range with considerable horizontal shear in the cross stream direction. The Rim Current structure in this segment during the simulation is essentially that of a quasi-stationary meander with five anticyclonic eddies in its shoreward side but with important developments during the simulation. The simulated current structure is in general agreement with several AVHRR

(Oğuz *et al.*, 1992) and CZCS (Sur *et al.*, 1994b) images analyzed to visualize the flow in this part of the basin. West of the Bosphorus Strait the Rim Current and the Coastal Current merge and flow eastward as a single structure following essentially the isobaths and separating from the coast at the Sakarya Canyon. The current turns sharply toward the coast forming a characteristic elbow and rejoins the coastal area just east of Baba Point. In this section a quasi-permanent anticyclone (Sakarya eddy) lies in the shoreward side of the current. Between Baba Point and Arkhangelsky Ridge the current meanders do not propagate and the meanders have wavelengths between approximately 80 to 125 km. During the course of the simulation, the center of the anticyclones displaces both along the coast ($O(50\text{ km})$) and offshore. The offshore displacement is reflected in the main pycnocline seaward of the 100 m isobath. In order to understand somewhat the dependencies of the Rim Current reflection around the Sakarya Canyon, simulations with modified winds and topography were performed. Simulations as the central simulation but without wind or twice the wind stress were performed. In the no wind case, a weaker Rim Current separates at the Canyon, returns after a shorter incursion in the deep water and upon return to the coast the Rim Current bifurcates, and it is partly entrained into the Sakarya eddy. If the wind stress is doubled, then a stronger current separates and does not re-attach to the coastal area. The latter has been observed in several occasions over the years. (See for instance Sur *et al.*, 1994b.) The difference in the behavior in the separation, we believe, is connected to the strength of the Rim Current just east of the Bosphorus Strait and not necessarily to the wind stress used here merely to modulate the current. This process, of some importance for exchanges between coastal and deep waters, requires detailed study. Simulations using the parameters of the central simulation, but with a smoother topography (see Section 3) are found to weaken the anticyclones originally supported by data. The convergence/divergence of the isobaths seems to be necessary for the maintenance of these eddies.

The vertical structure of the eddy generated downstream of the Sakarya Canyon is shown in Figure 9b. The quasi-stationary eddy attached to the coast in this area is known as the Sakarya eddy (Oğuz *et al.*, 1992). In the simulation, this eddy has a diameter of about 80 km, and it extends to about 300 m in the vertical. The eddy flow speed has a surface maximum and decreases gradually with depth. The volume transport of the Rim Current is about 3.3 Sv across this section. The 1 Sv transport increment with respect to the Rim Current transport in the vicinity of the Crimea peninsula can be attributed mostly to the merging of the Coastal Current and the Rim Current in the southwestern corner of the sea.

An important event in the simulation is the shedding of an anticyclonic eddy from the coastal area near Sinop (Fig. 9c). Day 21 (top panel) shows the typical configuration of the Anatolian Current meander. This meander remains in about the same position, gains strength, and forms a coastal eddy which subsequently detaches from the shelf. Once detached, it moves slightly to the west by day 45 (bottom panel). Latun (1990) reported the evolution of an anticyclonic eddy in the open sea, northwest of Sinop, observed during the summer of 1984. The evolution of the surface dynamic height referred to 500 db derived

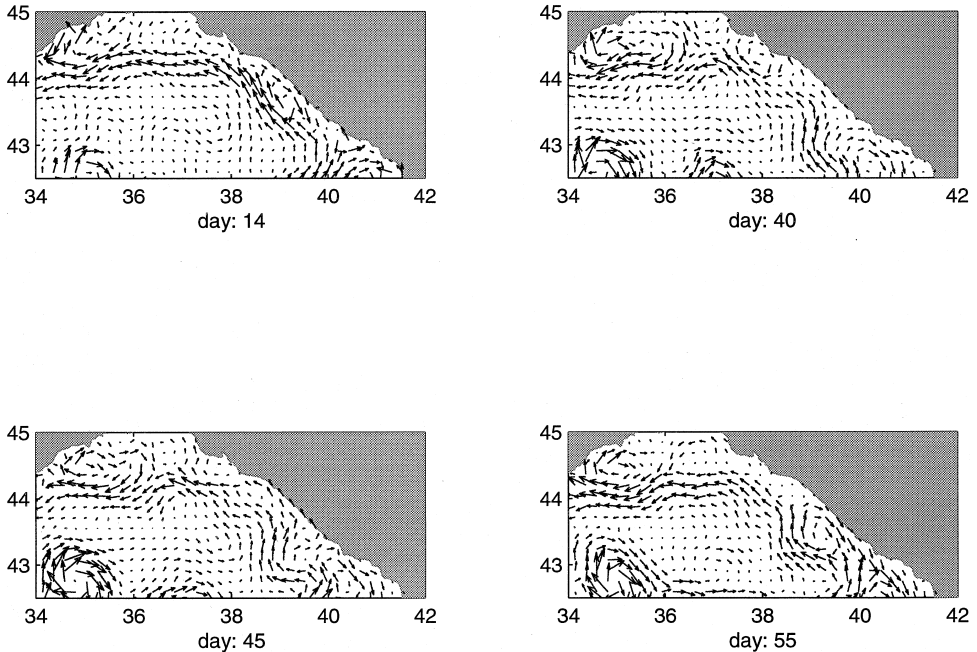


Figure 10. Caucasian-Kerch Current. (a) Surface velocity at day 14, 40, 45, 55. (b) Dynamic height (10^{-3} dyn m) at the sea surface from the data of the surveys: September 11–20, 1994 (upper panel), September 30–October 4, 1994 (lower panel), and the repeated survey of the northwestern eddy (dashed line) October 5–7, 1994. (Reproduced from Krivosheya *et al.*, 1998.)

from *in situ* hydrographic observations carried out between June and September 1984 is shown in Figure 9d. Compare the anticyclone observed near Sinop in June (Frame I in Fig. 9d) and the simulated detached ring in the bottom panel of Figure 9c. The presence of shelf water in the observed anticyclone core (Latun, 1990) indicates its origin. We hypothesize that the observed anticyclone was formed in a manner similar to the one noted in the simulation, namely a ring formation. This eddy exports a considerable amount of coastal water to the interior; therefore, the shedding of coastal eddies is a mechanism in the ventilation of the deep waters of the Black Sea.

Farther to the east the AC passes over the Arkhangelsky Ridge where the downstream flow meanders. The effect of the ridge can be seen clearly in Figure 6a. Farther downstream, the Rim Current separates from the coast and turns northward at 38E.

iii. Northeast circulation. Figure 10a is a time series of surface layer velocity in the northeastern region. The CKC is closer to the coast and narrower along the Caucasian coast than in other segments of the Rim Current, partly due to the very narrow shelf and a steep slope in this part of the basin. There is an ellipsoidal anticyclonic eddy located midway between Sukhumi and Novorossiysk. By day 40, this eddy has moved north toward the

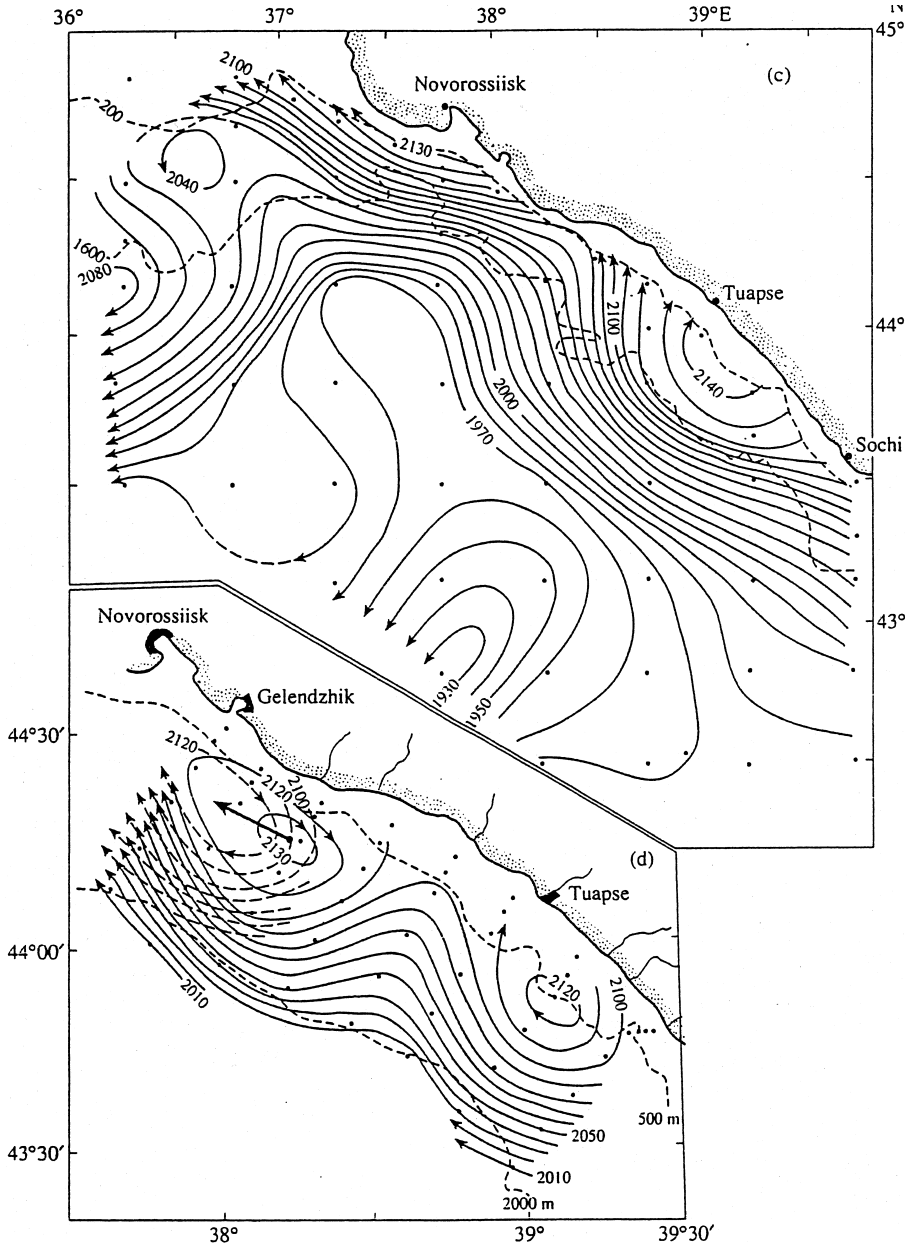


Figure 10. (Continued)

Kerch shelf area and weakens by day 55. The Batumi eddy is a complex of eddies, mostly anticyclonic and evolving relatively quickly $O(1 \text{ week})$. Occasionally, an anticyclonic eddy is shed from the Batumi eddy around Sukhumi between the coast and the CKC. The

eddy travels from the Sukhumi to the Novorossiysk area. Eddy shedding occurs about every 14 days. An eddy shed from the Batumi complex between days 40–45 progresses to the north along the coast. The eddy shed from the Batumi eddy at day 45 was moving northwest with the velocity of 4 km/day (from 42.2N and 39.5E to 43.4N and 39.2E). The CKC meanders very little outside of the segments interacting with passing anticyclones. Figure 10b shows the dynamic topography as estimated (Krivosheya *et al.*, 1998) for September 11–20, 1994 (upper panel) and September 30–October 4 (lower panel). Krivosheya *et al.* found that the eddies along the Caucasian coast had an elliptical shape with the length of the longitudinal axis of 35–45 km and the transversal axis of 25–35 km. These eddies were moving to the northwest at a velocity of 4–5 km per day. The long term current measurements in this area indicated passage of 32 eddies per year with approximately 40 km in size (Ovchinnikov *et al.*, 1994). The space and time variability of the eddies observed in this area correlate well with the model prediction described above. Blatov (1981) has proposed the formation and evolution of anticyclonic eddies to the combined effect of baroclinic stability, topographic constraint and topographic beta effects. Based on the model results, the CKC accommodates the passage of anticyclones shed by the Batumi eddy and under this circumstance the CKC possibly plays a secondary role in its dynamics. See Titov (1992) for a brief review on the observational evidence of anticyclones in the Caucasian region.

In the vicinity of Novorossiysk, the CKC bifurcates, with the main branch turning to the west and a weak flow to the north. Farther west an anticyclonic eddy forms. This anticyclone is known as the Crimea anticyclonic eddy and was not present in the data used for initialization. This eddy is generally observed during autumn (Oğuz *et al.*, 1993; 1994). The simulated eddy, once formed, remains until the end of the simulation (day 100).

iv. Barotropic circulation. The transport streamfunction had two different structures in the course of the simulation. Initially and up to day 10, the cyclonic cells in the deep water resemble barotropic basin modes. After equilibration, the strength of the cyclonic circulation in the western part of the deep basin is about twice that in the eastern part of the basin.

A characteristic synoptic structure of the transport streamfunction is shown in Figure 11. The barotropic circulation in the western sub-basin is stronger than in the eastern sub-basin. In addition, one observes tightening of the streamlines along the periphery. In the course of the simulation the intensification of the barotropic circulation along a relatively small segment $O(100\text{ km})$ of the Rim Current grows, moves in the direction of the current and then subsides. At any given time there are a few intensification zones. At the mesoscale scales, secondary cyclonic and anticyclonic develop on the meanders of the Rim Current. The configuration of the transport in the intensification zones is frontogenetic (Hoskins, 1982), and it tends to strengthen the Rim Current in these zones. The dynamical processes associated to the formation and evolution of these intensifications require study. The signature of the anticyclonic complexes is also evident in the barotropic transport. Finally, the evolution of the barotropic transport in the simulation does not conform to a

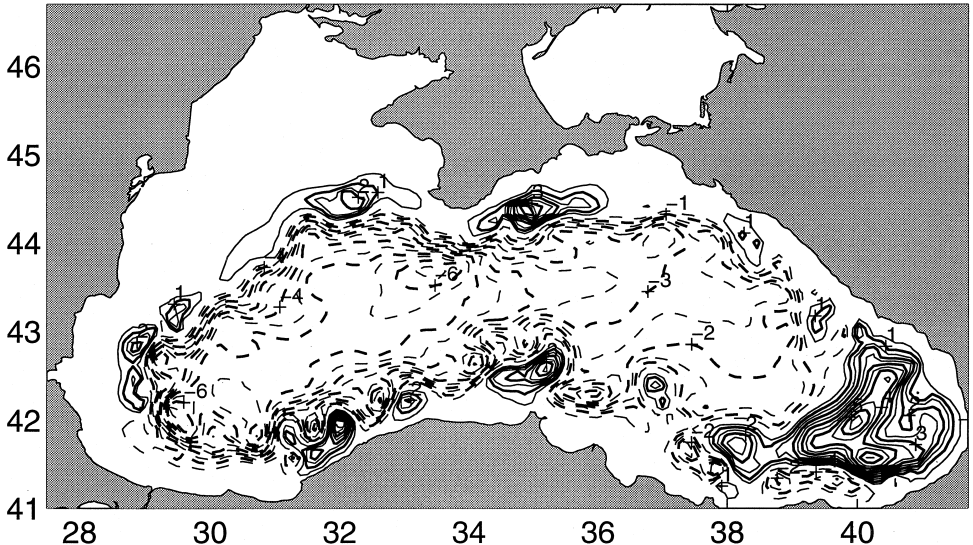


Figure 11. Barotropic transport at day 35. The cyclonic (positive, solid line) and anticyclonic (negative, dashed line) are approximately separated by the zero isoline, not shown here. Contour interval is 0.5 Sv (1 Sv = 10^6 m³/s).

simple level of no motion, especially in the steep slopes and in the passage of barotropic intensifications; thus, the rule of thumb of a level of no motion at 500 db should be considered as a rough first approximation in the estimate of the mesoscale velocity field.

5. Summary and discussion

The summer-autumn circulation of the Black Sea has been studied using data-driven simulations with a primitive equation model of the Harvard Ocean Prediction System. The four-dimensional fields yield a useful framework for the interpretation of data acquired during recent years by multi-institutional, multi-ship experiments in the Black Sea. The simulations have been used to identify mesoscale and sub-basin scale processes and interactions and they can now be used to set up pointed dynamical studies.

The results show that the model is able to generate and maintain the 3-d structures of the current, temperature and salinity fields. Model results are partially validated using observations. The size, structure and evolution of the main currents and eddies in simulation compare favorably to *in situ* observations and remotely sensed satellite measurements during the summer of 1992 and other summer seasons.

Observations and model simulations indicate at least three distinct regimes in the Rim Current associated to geographical regions: the Northwestern Slope Current, the Anatolian Current, and the Caucasian-Kerch Current. The structure of the main pycnocline at scales larger than 40 km is similar in these three segments of the Rim Current. The differences are

for the most part traceable to differences in topographic characteristics and upstream conditions. The northwestern slopes are relatively gentle with convergent and divergent isobaths. The Anatolian and Caucasian coasts are steep with narrow shelves. Current separation, and the formation of squirts and filaments are associated with abrupt orientation changes of the coastline, deep canyons and tall ridges in the bathymetry of the Anatolian coast (Fig. 8a); but they do not occur in the relatively gentler Caucasian coast. The weakening or absence of these circulation features in simulations with coarser bathymetry or coastline resolution were documented here, and in the work of Oğuz *et al.* (1995). For a related and informative sensitivity study in a coastal transition zone see Haidvogel *et al.* (1991). The Anatolian Current is connected to the Northwestern Shelf Break Current through the confluence zone to the west of the Bosphorus and it is connected to the Caucasian-Kerch Current through the Batumi anticyclonic complex. In addition to these current systems, there is also a well defined Coastal Current in the northwest shelf, the Anatolian coast and the Caucasian coast.

Different eddy structures were identified by means of their generation mechanisms and structures. The Sevastopol and Kaliakra eddies on the northwestern shelf break region are nearly stationary in the summer circulation. These eddies play a role in the transport of northwestern shelf surface waters to the deep basin. Eddies along the Anatolian coast are quasi-stationary and they propagate to the east very slowly. The detachment of an anticyclonic eddy near Sinop in the model (ring formation) may explain the origin of an observed anticyclonic eddy in the deep water. This process is an important mechanism in the ventilation of the deeper layers of the basin. The large-scale structure of the Batumi eddy does not change considerably in the simulation. This is in accordance with the observed historical data (Eremeev *et al.*, 1992). The Batumi anticyclone is actually a highly energetic system of anticyclonic eddies. About every 14 days the Batumi eddy sheds a coherent anticyclonic eddy that propagates northward between the coast and the Caucasian Kerch Current. This particular generation process of anticyclones in the Caucasian coast, found in the course of the numerical experiments, requires verification with observations and further study. The most rapidly changing eddies occur in the southwestern part of the basin as a result of the interaction between the Coastal Current and the Northwestern Shelf Break Current. The simulation produces highly variable cyclonic and anticyclonic eddies with 25–40 km diameter in this area.

The turbulent subgrid scale parameters, accuracy of bottom depth, horizontal resolution and initialization fields with nearly mesoscale resolution were found particularly important in the calibration of the central simulation presented here. A series of sensitivity analyses with different sets of the above parameters, except for the accuracy of bottom depth, did not change the general structure of the circulation features; but the strength and phase of the features are, in general, strongly dependent on these parameters.

Naturally, there are several important aspects of the circulation and dynamics that have been omitted. For instance, the role of coastal trapped waves, Kelvin waves, basin mode waves, etc. in the basin dynamics requires particular attention. For some recent work on

this issue in the Black Sea see Demirov (1994), Stanev (1990) and Stanev and Beckers (1999a). The relaxation of the rigid lid approximation will allow the study of the effects of gravity waves, in particular Kelvin waves, that we anticipate will play an important role, together with Rossby (basin) waves, in the dynamical adjustment of the sea.

Acknowledgments. The authors gratefully acknowledge Patrick Haley for modeling support and helpful comments and Vladimir Belokopytov from MSIA/URHI, Sevastopol, Ukraine for providing the wind dataset. The hydrographic CoMSBlack92 data were made available by the CoMSBlack Program and the NATO-SfP project. Şukru Beşiktepe was a visiting scientist at Harvard University while conducting this work. He was initially supported by TUBITAK (Turkish Scientific and Technical Research Council), the European Branch of the Office of Naval Research, and afterwards by TUBITAK under a joint NSF-TUBITAK program between Harvard University and the Middle East Technical University. The research of Carlos Lozano and Allan Robinson was supported by the Office of Naval Research under grant N00014-95-1-0371 and by NSF through the joint NSF-TUBITAK program.

REFERENCES

- Andersen, N. R. 1997. An early warning system for the health of the ocean. *Oceanography*, *10*, 14–23.
- Andrianova, O. R. 1997. The effect of seasonal and inter-annual variability of river run-off on the salinity of coastal waters in the north-western Black Sea. *Sov. J. Phys. Oceanogr.*, *8*, 117–122.
- Arakawa, A. 1996. Computational design for long-term numerical integration of the equations of fluid motion: Two-dimensional incompressible flow. Part I. *J. Comput. Phys.*, *1*, 119–143.
- Asselin, R. 1972. Frequency filter for time integrations. *Mon. Weather Rev.*, *100*, 487–490.
- Beckmann, A. and D. B. Haidvogel. 1993. Numerical simulation of flow around a tall isolated seamount: Part I: Problem formulation and model accuracy. *J. Phys. Oceanogr.*, *23*, 1736–1753.
- Blatov, A. S. 1981. Hydrological structure and energy supply for eddies in the Main Black Sea current. *Meteorologiya i gidrologiya*, *7*, 86–93.
- Blatov, A. S., N. P. Bulgakov, V. A. Ivanov, A. N. Kosarev and V. Tujilkin. 1984. Variability of the hydrophysical fields in the Black Sea. *Gidrometeoziad, Leningrad*, (in Russian) 240 pp.
- Bretherton, F. P., R. E. Davis and C. B. Fandry. 1976. A technique for objective analysis and design of oceanographic experiments applied to MODE-73. *Deep-Sea Res. II*, *40*, 539–582.
- Bulgakov, S. N. and V. M. Kushnir. 1995. Vertical structure of the current field in the northern Black Sea. *Oceanologia Acta*, *19*, 321–326.
- Caspers, H. 1957. Black Sea and the Sea of Azov, in *Treatise on Marine Ecology and Paleocology*, J. W. Hedgpeth, ed., Geological Society of America Memoir 72, Vol. 1, NY, 801–890.
- Demirov, E. K. 1994. Numerical model of the Black Sea eigenoscillations on a curvilinear boundary-fitted coordinate system. *Dyn. Atmos. Oceans*, *21*, 83–103.
- Demishev, S. G. and G. K. Korataev. 1966. Numerical modeling of synoptic variability of the Black Sea with considerations for seasonal boundary conditions. *Atmos. Ocean Phys.*, *32*, 108–116 (in Russian).
- Dukowicz, J. K., R. D. Smith and R. C. Malone. 1993. A reformulation and implementation of the Bryan-Cox-Semtner ocean model on the Connection Machine. *J. Atmos. Ocean. Technol.*, *10*, 195–208.
- Eremeev, V. N., L. M. Ivanov, S. V. Kochergin and O. V. Mel'nichenko. 1992. Seasonal variability and the types of currents in the upper layer of the Black Sea. *Sov. J. Phys. Oceanogr.*, *3*, 193–208.
- Eremeev, V. N. and V. M. Kushnir. 1996. The layered structure of currents and vertical exchange in the Black Sea. *Oceanology*, *36*, 9–15.

- Filippov, D. M. 1966. Circulation and water structure of the Black Sea. NAUKA, Moscow, 136 pp. (in Russian).
- Gamsakhurdiya, G. R. and A. S. Sarkisyan. 1976. Diagnostic calculations of the current velocities of the Black Sea. *Oceanology*, 15, 164–167 (in Russian).
- Ginsburg, A. I., E. A. Kontar, A. G. Kostyanio, V. G. Krivosheya, D. M. Solov'ev, S. V. Stanichnyi and S. Yu. Laptev. 1999. System of synoptic eddies over a sharp bottom slope in the northwestern part of the Black Sea in summer 1993 (satellite and ship data). *Oceanology*, 38, 51–58.
- Grigor'ev, A. V., V. A. Ivanov and N. A. Kapustina. 1996. Correlation structure of the Black Sea thermohaline fields in the Summer season. *Oceanology*, 36, 334–338.
- Haidvogel, D. B., A. Beckman and K. S. Hedström. 1991. Dynamical simulations of filament formation and evolution in the coastal transition zone. *J. Geophys. Res.*, 96, 15017–15040.
- Haley, P. J., Jr. 1996. GRIDS. Harvard Open Ocean Model Reports, 54, Harvard University, Cambridge, MA.
- Haley, P. J. and C. J. Lozano. 1999. COND-TOPO: Topographic conditioning in MATLAB. Harvard Open Ocean Model Reports, 61, Harvard University, Cambridge, MA.
- Hill, A. E. 1998. Buoyancy effects in coastal and shelf seas, *in* The Sea. The Global Coastal Ocean: Processes and Methods, A. R. Robinson and K. Brink, eds., Vol. 10, John Wiley and Sons, NY, 21–62.
- Hoskins, B. J. 1982. The mathematical theory of frontogenesis. *Ann. Rev. Fluid Mech.*, 14, 131–151.
- Klinger, B. A. 1994. Inviscid current separation from rounded capes. *J. Phys. Oceanogr.*, 24, 1805–1811.
- Krivosheya, V. G., I. M. Ovchinnikov, V. B. Titov, V. G. Yakubenko and A. Yu. Skirta. 1998. Meandering of the main Black Sea current and eddy formation in the northeastern part of the Black Sea in Summer 1994. *Oceanology*, 38, 492–498.
- Latun, V. S. 1990. Anticyclonic eddies in the Black Sea in the summer of 1984. *Sov. J. Phys. Oceanogr.*, 1, 279–286.
- Lermusiaux, P. F. J. 1999. Estimation and study of mesoscale variability in the Strait of Sicily. *Dyn. Atmos. Oceans*, 29, 130–135.
- Lozano, C. J., A. R. Robinson, H. G. Arango, A. Gangopadhyay, N. Q. Sloan, P. J. Haley and W. G. Leslie. 1996. An interdisciplinary ocean prediction system: Assimilation strategies and structured data models, *in* Modern Approaches to Data Assimilation in Ocean Modelling, P. Malanotte-Rizzoli, ed., Elsevier Oceanography Series, Elsevier Science, 413–456.
- Lozano, C. J., P. J. Haley, H. G. Arango, N. Q. Sloan and A. R. Robinson. 1994. Harvard coastal/deep water primitive equation model. Harvard Open Ocean Model Reports, 52, Harvard University, Cambridge, MA, 15 pp.
- Mee, L. D. 1992. The Black Sea in crisis: the need for concerted international action. *Ambio*, 24, 278–286.
- Oğuz, T., D. G. Aubrey, V. S. Latun, E. Demirov, L. Koveshnikov, H. İ. Sur., V. Diaconu, Ş. Beşiktepe, M. Duman, R. Limeburner and V. Eremeev. 1994. Mesoscale circulation and thermohaline structure of the Black Sea observed during HydroBlack'91. *Deep-Sea Res.*, 41, 603–628.
- Oğuz, T. and Ş. Beşiktepe. 1999. Observation on the Rim Current structure, CIW formation and transport in the western Black Sea. *Deep-Sea Res.*, 46, 1733–1753.
- Oğuz, T., Ş. Beşiktepe, Ö. Baştürk, İ. Salihoğlu, D. Aubrey, A. Balci, E. Demirov, V. Diaconu, L. Dorogan, M. Duman, L. Ivanov, S. Kononov, S. Stayanov, S. Tuğrul, V. Vladimirov and A. Yilmaz. 1993. CoMSBlack'92a, Report on the Physical and Chemical Intercalibration Workshop, 15–29 January 1993. Comsblack 93-012 Technical Report, Institute of Marine Sciences, METU, Erdemli, Turkey.
- Oğuz, T., Ş. T. Beşiktepe, L. I. Ivanov and V. Diaconu. 1998. On the ADCP derived Rim Current

- structure, CIW formation and the role of mesoscale eddies on the CIW transport in the Black Sea, *in* NATO TU-Black Sea Project: Ecosystem Modelling as a Management Tool for the Black Sea, L. Ivanov and T. Oğuz, eds., Vol. 2, Kluwer Academic Publishers, Netherlands, 93–118.
- Oğuz, T., H. Ducklow, P. Malanotte-Rizzoli, S. Tugrul, N. Nezlin and U. Ünlüata. 1996. Simulation of annual plankton productivity cycle in the Black Sea by a one-dimensional physical-biological model. *J. Geophys. Res.*, *101*, 16585–16599.
- Oğuz, T., V. S. Latun, M. A. Latif, V. V. Vladimirov, H. İ. Sur, A. A. Markov, E. Özsoy, B. B. Kotovshchikov, V. V. Eremeev and Ü. Ünlüata. 1993. Circulation in the surface and intermediate layers of the Black Sea. *Deep-Sea Res. I*, *40*, 1597–1612.
- Oğuz, T., P. La Violette and U. Ünlüata. 1992. Upper layer circulation of the southern Black Sea: Its variability as inferred from hydrographic and satellite observations. *J. Geophys. Res.*, *97*(C8), 12569–12584.
- Oğuz, T. and P. Malanotte-Rizzoli. 1996. Seasonal variability of wind and thermohaline driven circulation in the Black Sea. *J. Geophys. Res.*, *101*(C7), 16551–16569.
- Oğuz, T., P. Malanotte-Rizzoli and D. Aubrey. 1995. Wind and thermohaline circulation of the Black Sea driven by yearly mean climatological forcing. *J. Geophys. Res.*, *100*, 6845–6863.
- Ovchinnikov, I. M., V. B. Titov and V. G. Krivosheya. 1994. Major fluid dynamical processes and their role in the ecology of waters of the Black Sea. *Oceanology*, *33*, 707–712.
- Ovchinnikov, I. M. and Yu. I. Popov. 1987. Evolution of the cold intermediate water in the Black Sea. *Oceanology*, *27*, 555–560.
- Özsoy, E. and U. Ünlüata. 1998. The Black Sea, *in* The Sea. The Global Coastal Ocean: Processes and Methods, A. R. Robinson and K. Brink, eds., Vol. 10, John Wiley and Sons, NY, 889–914.
- Pacanowski, R. C. and S. G. H. Philander. 1981. Parameterization of vertical mixing in numerical models of tropical oceans. *J. Phys. Oceanogr.*, *11*, 1443–1451.
- Robinson, A. R., P. F. J. Lermusiaux and N. Q. Sloan. 1998. Data Assimilation, *in* The Sea. The Global Coastal Ocean: Processes and Methods, A. R. Robinson and K. Brink, eds., Vol. 10, John Wiley and Sons, NY, 541–594.
- Robinson, A. R., J. J. McCarthy and B. J. Rothschild. 1999. Interdisciplinary ocean science is evolving and a systems approach is essential. *J. Mar. Syst.*, *22*, 231–239.
- Sarkisyan, A. S. and V. F. Ivanov. 1971. The joint effect of baroclinicity and bottom relief as an important factor in dynamics of sea flows. *Izv. Acad. Sci. USSR Atmos. Oceanic Phys.*, *7*, 173–188.
- Shapiro, R. 1970. Smoothing, filtering and boundary effects. *Rev. Geophys. Space Phys.*, *8*, 359–387.
- Shi, C. and S.-Y. Chao. 1994. Eastward jets over diverging isobaths, with applications to the Gulf Stream past the Grand Banks. *J. Geophys. Res.*, *99*, 22689–22706.
- Sloan, N. Q. 1996. Dynamics of a shelf-slope front: Process studies and data-driven simulations in the Middle Atlantic Bight. PhD thesis, Harvard University, Cambridge, MA, 230 pp.
- Spall, M. A. and A. R. Robinson. 1990. Regional primitive equation studies of the Gulf Stream Meander and Ring Formation Region. *J. Phys. Oceanogr.*, *20*, 985–1016.
- Stanev, E. V. 1990. On the mechanisms of the Black Sea circulation. *Earth-Science Reviews*, *28*, 285–319.
- Stanev, E. V. and J. M. Beckers. 1999a. Barotropic and baroclinic oscillations in strongly stratified ocean basins: Numerical study of the Black Sea. *J. Mar. Syst.*, *19*, 65–112.
- _____. 1999b. Numerical simulations of seasonal and interannual variability of the Black Sea thermohaline circulation. *J. Mar. Syst.*, *22*, 241–267.
- Sur, H. İ., E. Özsoy and U. Ünlüata. 1994a. Boundary current instabilities, shelf mixing and eutrophication processes in the Black Sea. *Progr. Oceanogr.*, *33*, 249–302.

- _____. 1994b. Boundary current instabilities, upwelling, shelf mixing and eutrophication processes in the Black Sea. *Progr. Oceanogr.*, 33, 249–302.
- Sur, H. İ. and Yuri P. Ilyin. 1997. Evolution of satellite derived mesoscale thermal patterns in the Black Sea. *Progr. Oceanogr.*, 39, 109–151.
- Titov, V. B. 1980. Character of the circulation and vertical structure of currents in the eastern part of the Black Sea. *Oceanology*, 20, 279–282.
- _____. 1992. On the role of eddies in the formation of the current regime on the Black Sea shelf and in the ecology of the coastal zone. *Oceanology*, 32, 24–30.
- Ünlüata, U., D. G. Aubrey, Z. Belberov, A. Bologna, V. Eremeev and M. Vinogradov. 1993. International program investigates the Black Sea. *EOS*, 36, 408–412.
- Ünlüata, U., T. Oğuz, M. A. Latif and E. Özsoy. 1990. On the physical oceanography of the Turkish straits, *in* *The Physical Oceanography of Sea Straits*, L. J. Pratt, ed., NATO/ASI Series, Kluwer, Dordrecht. The Netherlands, 25–60.

Received: 27 July, 2000; revised: 24 May, 2001.